Dalton Transactions

RSCPublishing

PERSPECTIVE

Key Multi(Ferrocenyl) Complexes in the Interplay between Electronic Coupling and Electrostatic Interaction

Cite this: *Dalton Trans.*, 2014, 00, 00

Received ooth xxxx 2014,
Accepted ooth xxxx 2014

DOI: 10.1039/xoxx00000x

www.rsc.org/

Saverio Santi,[a,*] Annalisa Bisello,[a] Roberta Cardena[a] and Alessandro Donoli[b]

In this review, the properties of the most significant examples of multi(ferrocenyl) cations containing a number of ferrocenyl units from two to six will be discussed and the results compared with the outcomes of some our recent works on conjugated ferrocenyl complexes, trying to give an overview on how the nature of the bridging ligand, the distance among the redox-active centres and the medium affect the electronic and electrostatic properties of the molecules.

[a] *Department of Chemical Sciences, University of Padova, 35131 Padova, Italy*
[b] *Luxottica S.r.l. Via Valcozzena 10, 32021 Agordo (BL), Italy*

Introduction

The preparation of multicomponent molecular systems with specific redox, optoelectronic, magnetic, and conductive properties is currently fundamental for modern technology.[1]

Among metallocene-based metallorganic structures,[2] multi(ferrocenyl) compounds were suggested as potential candidates for molecular electronics due to their well-defined and robust redox properties.[3]

Indeed, multi(ferrocenyl) complexes with conjugated spacer groups and displaying multielectron redox chemistry are of particular interest owing to their characteristics due to unpaired electron density migration properties of their mono-oxidised derivatives .[4] These switchable arrays were intensely studied because conjugated organic chains containing Fe^{II}/Fe^{III} couples of the ferrocenyl group can be potentially used as quantum cellular automata, optoelectronic materials for application in redox or photonic devices.[5]

Many of these ferrocenyl derivatives belong to the family of mixed-valence complexes in which at least two equivalent ferrocenyl units electronically interact and the Fe^{II}/Fe^{III} oxidation states coexist in the same molecule. The mixed-valence systems are excellent benchmarks for the investigation of the electronic interactions.[6] Actually, in multi(ferrocenyl) complexes the formation of mixed-valence intermediates is often responsible for the aforesaid properties.

The synthesis of the Creutz-Taube[7] mixed-valence ions encouraged the investigations on a series of coordination complexes in order to establish the way in which two or more metals linked by nitrogen (or other heteroatoms) containing bidentate ligands.[8]

Concomitantly, Cowan and co-workers focused their research on different diferrocenyl complexes,[9] establishing the crucial role of the ferrocenyl moiety in the mixed-valence field.

Bimetallic and multimetallic complexes are often precursors of mixed-valence species generated by chemical or electrochemical activation and several reviews have been devoted to this topic.[10] The redox, optical and magnetic properties of these compounds depend on the extent of the metal–metal interaction among the metals.

In this Perspective article, the electronic and electrostatic properties of, to our opinion, the key multi(ferrocenyl) cations containing a number of ferrocenyl units from two to six will be discussed. Some of our recent works on conjugated ferrocenyl complexes will be considered and compared with the most significant examples reported in literature. We will try to give a comparative overview on how the nature of the bridging ligand, the distance among the redox-active centres, and the medium affect the electronic and electrostatic properties of the molecules.

Particular attention will be devoted to the bis(ferrocenyl) and tris(ferrocenyl) derivatives, showing as the latter should provide the means of bridging the gap between the interpretation of the related charge and electron transfer processes in simple bimetallic molecules and that in multicomponent systems.

A validation for this experimental evidence arises predominantly from the classification proposed by Robin and Day[11] and the classical Marcus-Hush theory.[12]

Theoretical aspects

According to Robin and Day, mixed-valence species are ordered into three classes, depending on the extent of charge transfer or delocalization. The strength of electronic interaction between the oxidized and reduced sites ranges from essentially zero (Class I) to weakly or moderate (localized valence, Class II), to very strong electronic coupling (delocalized valence, Class III).

For a moderate coupled, class II, bimetallic system, the mixed-valence situation is described by the equilibrium between two ground states involving trapped-valence systems (Class II), in which

a vectorial electron transfer from M_1 to M_2 occurs and vice versa (eq. 1):

$$M_1^{+}\!\sim\!M_2 \rightleftharpoons M_1\!\sim\!M_2^{+} \quad (1)$$

The accessibility of the charge delocalized transition state (or excited state) allows the occurrence of the intervalence charge transfer (IVCT), i.e. a metal-to-metal charge transfer (MMCT). In the case of a delocalized, class III, bimetallic system, there is no thermal barrier to electron transfer and the two metal ions hold formally averaged oxidation state in the ground state, that is 2.5 for a mono-oxidised bis-iron(II) complex. The actual situation is a resonance between two mesomeric structures (eq. 2):

$$M_1^{+}\!\sim M_2 \longleftrightarrow M_1\!\sim\!M_2^{+} \quad (2)$$

Thus, the MMCT transition corresponds to an electron density distribution within the metal centred orbital(s) and the rate of the electron transfer is representable as electron mobility within this orbital(s).[13]

Intramolecular metal-to-metal electron transfer can be theoretically inspected using the classical model introduced by Marcus. [12f–i] According to Marcus, the potential energy surface of a degenerate mixed-valence system can be described by two parabolic curves, $G_a = \lambda q^2$ and $G_b = \lambda(1-q)^2$, which represent the non-interacting (diabatic) states as a function of a global reaction coordinate "q". The electronic coupling of these two diabatic states corresponds to the electronic wavefunction mixing and produces two interacting (adiabatic) surfaces of energy G_1 (ground state) and G_2 (excited state), avoiding crossing in the intersection region. The schematic representation for a bimetallic complex is drawn in Fig. 1.

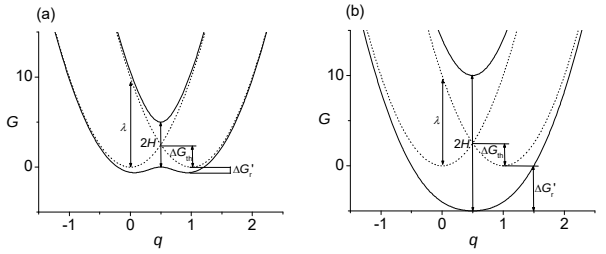

Fig. 1 The adiabatic (G_1 and G_2, solide lines) and diabatic energy surfaces (G_a and G_b, dashed line) for (a) localized class II and (b) delocalized class III systems for an isoergonic complex. $\Delta G_r' = \Delta G_r / 2$ represents the resonance free energy per mixed-valence complex, where ΔG_r accounts for the free energy of resonance exchanges.

The two metal groups represent the donor and the acceptor, i.e. the two sites between which electron transfer occurs, and they are connected by an organic spacer (or bridging ligand); the molecule is surrounded by a solvation sphere, the equilibrium polarization of which is generally different before and after the electron transfer. The energy cost due to geometry modifications to go from a neutral to a charged metal centre (and vice versa) is called reorganization energy, λ.

Hush applied the Marcus theory to the issue of intervalence transitions.[12a–e, 14] The energy surface for thermal electron transfer is obtained from a two-state classical model in which the electronic interaction between diabatic surfaces is the off-diagonal matrix element H in a 2×2 secular determinant. The solution gives eq. 3 which allows calculating the adiabatic energy surfaces represented in Fig.1 in which the surface splitting at the avoided intersection results twice the value of electronic coupling H:

$$G_1 = \frac{1}{2}\{(G_b + G_a) - [(G_b - G_a)^2 - 4H^2]^{1/2}\} \quad (3a)$$

$$G_2 = \frac{1}{2}\{(G_b + G_a) + [(G_b - G_a)^2 - 4H^2]^{1/2}\} \quad (3b)$$

For a weakly coupled Class II system, when the surface splitting is smaller than the reorganization energy ($2H << \lambda$), the vertical separation is almost equal to λ (Fig. 1a). The electronic mixing H causes the appearance of a double minimum adiabatic surface in the ground state with a maximum corresponding to the thermal electron transfer barrier $\Delta G^{\neq}$ given by eq. 4:

$$\Delta G^{\neq} = \frac{\lambda}{4} - H + \frac{H^2}{\lambda} \quad (4)$$

Two electron transfer paths are viable: (i) the thermal process where the system moves from one minimum of the low lying adiabatic surface over the energy barrier $\Delta G^{\neq}$; (ii) the optical process where a vertical transition promotes the system from one minimum of the lower adiabatic surface to the upper adiabatic surface.

Experimental techniques

1. Near infrared spectroscopy

A powerful probe for evaluating the magnitude of the metal–metal interaction in mixed-valence compounds involves analysis of the intervalence charge transfer (IVCT) absorption in near infrared (NIR) region. The maximum energy of this IVCT transition is $\tilde{\nu}_{max} = \lambda$ and is usually observed as a low energy and broad band in the NIR spectrum.

In the case of strongly coupled class III systems, the surface splitting is greater than the reorganization energy ($2H >> \lambda$), the resulting adiabatic ground-state surface displays a single minimum and $\Delta G^{\neq}$ disappears at $H = \lambda/2$, as predicted by eq. 4. The odd electron is now delocalized between the metal centres and $\tilde{\nu}_{max} = 2H$ (see Fig.1b).

For a class II system, Hush theory deduces the relationships associated to the characteristics of the IVCT band (eqs. 5–7). The energy of the intervalence band is predicted to be dependent of $\Delta G^{\neq}$ (eq. 5):

$$\tilde{\nu}_{max} = 4\Delta G^{\neq} \quad (5)$$

The magnitude of H is related to the maximum energy $\tilde{\nu}_{max}$, the molar absorption coefficient ε_{max}, the half-bandwidth $\Delta\tilde{\nu}_{max}$ of the IVCT absorption, and the true electron transfer distance r:

$$H = \frac{0.0206}{r}\sqrt{\tilde{\nu}_{max}\Delta\tilde{\nu}_{1/2}\,\varepsilon_{max}} \quad (6)$$

When the electronic coupling is pronounced, r can be considerably shorter than the geometric distance r_g. The value of $\Delta\tilde{\nu}_{max}$ for a localized mixed-valence system is predicted by eq. 7,

$$\Delta\tilde{\nu}_{1/2} = \sqrt{16RT\ln 2\,\tilde{\nu}_{max}} \quad (7)$$

that at the limit of high temperature ($H >> k_B T$, T = 298 K) gives eq. 8:

$$\Delta\tilde{\nu}_{1/2}\ (cm^{-1}) = \sqrt{2310\,\tilde{\nu}_{max}} \qquad (8)$$

Two fundamental reviews on the application of Hush theory to mixed-valence complexes of transition metal centres are those by Creutz[15] and by Crutchley[16]. Eq. 7 and 8 are valid only for Gaussian-shaped bands and a rigorous quantum chemical formulation was given by Cave, Newton and Sutin[17]

The assignment of a bimetallic mixed-valence system to class II or class III is usually based on the comparison between the experimental half-bandwidth and that calculated by mean of eq. 7. If the values are similar, the valence state is considered class II; if the experimental bandwidth is smaller, it is class III.[15,16,18] In addition, the effect of solvent on the mixed-valence properties has often been used to distinguish between class II or III complexes.[1,2,7] In fact, if the rate of the electron transfer between donor and acceptor is smaller than the rate of solvent relaxation (10^{12} s^{-1}), $\tilde{\nu}_{max}$ is predicted to be linear with the solvent parameter ($1/n^2 - 1/\varepsilon_o$) by the classical two-state Hush theory. [12a–e] A blue shift of the band energy of a class II mixed-valence derivative is experimentally observed by increasing the quantity $1/n^2 - 1/\varepsilon_o$ and the odd electron is trapped on one metal. Conversely, the energy of the intervalence transition of a class III system is expected to be solvent-independent.

More recently, Meyer[19] has defined borderline class II/class III systems which exhibit both localized and delocalized behaviours. Meyer stated that, if the rate of the electron transfer is greater than the rate of solvent relaxation, $\tilde{\nu}_{max}$ of the mixed-valence complex appears solvent independent even though the odd electron is trapped on one metal in the electronic time scale 10^{15} s^{-1}. For a borderline Class II/Class III mixed-valence species, when the thermal barrier $\Delta G^{\neq}$ is vanished and $\tilde{\nu}_{max} = \lambda$, the electronic coupling H is equal to $\tilde{\nu}_{max}/2$.

Brunschwig, Creutz and Sutin proposed a criterion based on the observed and calculated half-bandwidths,[14b] according to eq. 9:

$$\Gamma = 1 - (\Delta\tilde{\nu}_{1/2})_{obsd} / (\Delta\tilde{\nu}_{1/2})_{calcd} \qquad (9)$$

The value of Γ aids in classifying a mixed-valence species: for weakly coupled class II systems $0 < \Gamma < 0.1$, for moderately coupled class II systems $0.1 < \Gamma < 0.5$, for borderline class II/class III systems $\Gamma \approx 0.5$, and for delocalised class III systems $\Gamma > 0.5$.

2. Electrochemistry

Besides the optical techniques, electrochemistry is a powerful tool to inspect on the thermodynamic stability of mixed-valence systems and is frequently employed to predict the magnitude of metal-metal electronic interaction.

The thermodynamic stability of the mixed-valence state can be easily calculated from electrochemical data. The comproportionation constant K_c for the equilibrium described by eq. 10 is given by $K_c = \exp(F\Delta E/RT)$ where ΔE is the oxidation potential difference between the first and second oxidation of a bimetallic complex measured by mean of cyclic voltammetry (CV), differential pulse voltammetry (DPV) and square wave voltammetry (SWV).

$$M_1\sim\sim M_2 \ + \ M_1^{+}\sim\sim M_2^{+} \ \rightleftharpoons \ 2\,[M_1\sim\sim M_2]^{+} \qquad (10)$$

The nature of the spacer connecting two or multiple redox units has a relevant role in modulating ΔE separations.

Larger and resolvable separations are indicative of increased K_c values, corresponding to greater thermodynamic stability of the mixed-valence state. The determination of the ΔE value allows evaluating the related stabilization energy $\Delta G_c = -F\Delta E$. Different energy factors contribute to the magnitude of ΔG_c:

$$\Delta G_c = -F\Delta E = \Delta G_s + \Delta G_e + \Delta G_i + \Delta G_r + \Delta G_{ex} + \Delta G_{ip} \qquad (11)$$

According to Sutton and Taube[20], for most of mixed-valence complexes the first four factors mainly contribute to the magnitude of ΔG_c. In eq. 11, ΔG_s reflects the statistical distribution of the comproportionation distribution: in an electrochemical experiment with a molecule containing n noninteracting equivalent redox centres, one should observe a separation of $(RT/F)\times\ln(2)^n$ (for $n = 2$ $\Delta E = 36$ mV, $K_c = 4$, $\Delta G_s = 3.5$ kJ at 298 K),[21] a rather smaller value than that measurable with the common electrochemical techniques. ΔG_e represents the electrostatic repulsion of two charge metal centres, ΔG_i is the inductive factor dealing with the competitive coordination of the bridging ligand by the metal ions, and ΔG_r accounts for the free energy of resonance exchanges, the only contribution to ΔG_c denoting real metal-metal coupling. Sutin and Crutchley[8b] pointed out early that another term, ΔG_{ex}, must be considered if antiferromagnetic exchange significantly stabilizes the doubly oxidized reactant complex of eq. 10. However, in systems where superexchange occurs via the electron transfer pathway, the magnitude of ΔG_{ex} should be small or insignificant. Finally, Geiger has shown that ion pairing can have a strong effect on ΔG_c and the ion- pairing factor ΔG_{ip} either increases or decreases its magnitude depending on the charge of the complexes in eq. 10. The magnitude of ΔE has been frequently interpreted as a measure of the interaction between the metals. However, a cautionary warning on the use of the electrochemical data is required. In particular, the medium properties, i.e. the dielectric constant or the donor number of the solvent together with the nucleophylicity or ion-pairing ability of the supporting electrolyte can dramatically modify ΔG_c.[22]

The importance of the electrostatic interaction was demonstrated by Sutton and Taube[20]: by evaluating the electronic contribution by mean of the Hush analysis, they established that the electrostatic effect explains most of the observed stabilization energy of the mixed-valence state. This means that electrochemical separations (ΔE) may be observed in the absence of any electronic interactions. On the other hand, an undetectable or small ΔE is not diagnostic of a negligible communication, since even in the case where a single electrochemical wave is observed a significant amount of mixed-valence species may be present in solution.[20,23]

The dependence of K_c on metal-metal distance was discussed by Hush.[24] When the metal centres are separated by a large distances, K_c becomes smaller and becomes more difficult to measure. It is possible to estimate K_c by using a simple theory considering that the deviation of K_c from the entropic factor of 4 is due to the electrostatic repulsion energy of the metal charges. Thus, a plot of $\ln K_c$ *vs* $1/r_g$ (r_g is the geometric distance) should be linear and pass through $K_c = 4$ for $1/r_g \rightarrow 0$.

The only factor of ΔG_c which accounts for "real" metal-metal coupling is ΔG_r. We can break[25] ΔG_c into two contribution (eq. 12), ΔG_{nr} which include all the nonresonance factors, and the resonance free energy ΔG_r:

$$\Delta G_c = \Delta G_{nr} + \Delta G_r \qquad (12)$$

In the case of a symmetrical weakly coupled class II complex, it has been shown[25] that the resonance stabilization is given by eq. (13):

$$\Delta G_r = \frac{2H^2}{\lambda} = \frac{2H^2}{\tilde{\nu}_{\max}} \quad (13)$$

For a class III complex ΔG_r is predicted by eq. 14:

$$\Delta G_r = 2\left(H - \lambda/4\right) = \tilde{\nu}_{\max} - \lambda/2 \quad (14)$$

It obviously results that $\Delta G_r = \tilde{\nu}_{\max}/2$ for a borderline system ($H \approx \lambda$) and $\Delta G_r \rightarrow \tilde{\nu}_{\max}$ for very strongly coupled systems ($H >> \lambda$).

Bis(ferrocenyl) complexes

The series of bis(Ferrocenyl) polyenes of general formula $Fc(CH{=}CH)_nFc$ (**1a–e**, n = 1–6), prepared by Launay and Spangler, offered a unique opportunity to study accurately the intervalence electron transfer and the decay law of the electronic interaction with distance. The study of the mixed-valence species obtained by monoxidation of **1a–e** showed that intervalence transition appeared at markedly low energy, and metal–metal electronic coupling existed even when the ΔE splitting was not observed (n = 4–6).[26]

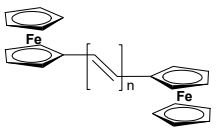

1a-e: n = 1- 6

As expected, a plot of ln K_c *vs* 1/ r_g was found linear and passed through $K_c = 4$ for $1/r_g \rightarrow 0$ (Fig. 2a). The electrostatic interaction between the metal charges is the major effect in these compounds where the metal centres are separated by a large distance (7-18 Å). Describing the intermetallic coupling by using the two-state model, if this coupling is small, as it must be in order that this model is appropriate,[12a] the Hush model allows H to be calculated from the parameters of the deconvoluted intervalence band (eq. 6).

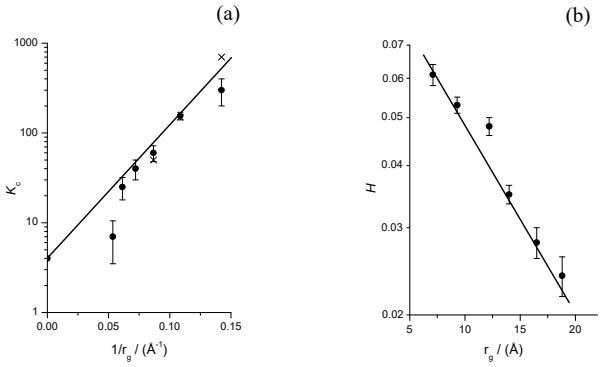

Fig. 2 (a) Comproportionation constant K_c (log scale) as a function of $1/r_g$: (●) from redox titration; (⊗) from wave splitting. (b) Metal-metal coupling (log scale) H as function of r_g in the hypothesis of a *trans* configuration of terminal ferrocene groups.

From McConnell's theory,[27] the coupling should decrease exponentially as n increases according to eq. 15:

$$H_n = H_0 e^{-\gamma n} \quad (15)$$

where γ is defined as a measure of the coupling drop. As far as the decay of the metal-metal coupling with distance along the series **1a–e**, the plot of ln$H$ was found almost linear indicating that H decays exponentially with distance (Fig. 2b). The slope is 0.087 Å^{-1}, corresponding to a decrease of a factor 2 for each 8 Å.

The isomeric complexes *E*- (**2b**) and *Z*-1,2-bis(1'-ethyl- l-ferrocenyl)-1,2-dimethylethylene (**3b**) were reported by Dong and Peng. The complexes **2** and **3** provided the opportunity to study the intervalence electron transfer between two ferrocenyl groups as a function of the relative orientation and separation of donor and acceptor. However, the surprisingly similar optical properties found for weakly coupled $\mathbf{2b}^+$ and $\mathbf{3b}^+$ mixed-valence isomers, together with the electrochemical measurements of **2b** and **3b**, indicated that electron transfer is associated with $E \rightleftarrows Z$ isomerization. Indeed, the solutions obtained by chemical reduction of the dioxidized cations and of the mixed-valence solutions showed both *E* and *Z* isomers. The isomerization was not observed in a solution of neutral complexes. Possibly, the isomerization is associated with thermal electron transfer or photoinduced electron transfer through the π* orbital of ethene bridge in mixed-valence or dioxidized cations.

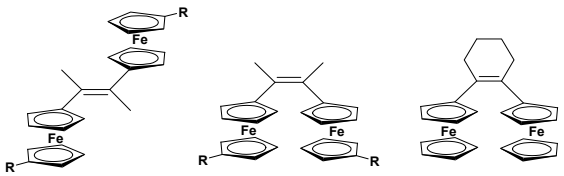

2a: R = H
2b: R = C_2H_5

3a: R = H
3b: R = C_2H_5

4

In order to circumvent isomerization problems, the complexes **2a** and **3a** and the related 1,2-diferrocenyl-cycloexene (**4**) were prepared by Kwan. The stability of their mixed-valence derivatives and of **4** was discussed mainly in terms of resonance delocalization and electrostatic repulsion energy. According to Hush analysis, the energy contribution due to the electrostatic repulsion dominates the overall stability of the mixed-valence state in $\mathbf{2a}^+$, $\mathbf{3a}^+$, and $\mathbf{4}^+$, while the resonance delocalization contributes less than 4%.

The *ortho* (**5o**), *meta* (**5m**) and *para* (**5p**) isomers of bis(ferrocenyl)benzene were prepared by Launay and Joachim.[28]

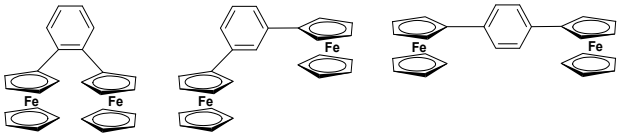

5o **5m** **5p**

An experimental and theoretical study of the effect of topology on intervalence electron transfer was accomplished. Except for **5m**, for which a single oxidation wave appeared whatever the electrochemical technique was used, the beginning of splitting was observed for **5o** and **5p**. Adapting a literature procedure,[21b] ΔE and K_c values were determined simulating the profiles of DPV measurements. Among the energetic factors which contribute to K_c

values, the electrostatic interaction, strongly related to the distance between the redox centres, was assumed to be predominant. Indeed, the *ortho* isomer **5o** showed the highest K_c value but the *meta* isomer **5m**, having the intermediate iron–iron distance, provided the smallest K_c value, indicating that the electrostatic interaction is not sufficient to explain K_c variations. Despite the small ΔE splitting for $\mathbf{5o}^+$ (131 mV), $\mathbf{5p}^+$ (104 mV) and $\mathbf{5m}^+$ (90 cm^{-1}), intervalence transitions for these compounds were detected and the values of metal–metal couplings H, calculated from the intervalence band parameter using Hush's relalationship (eq. 6), resulted in the order $\mathbf{5p}^+$ (347 cm^{-1}) > $\mathbf{5o}^+$ (202 cm^{-1}) > $\mathbf{5m}^+$ (161 cm^{-1}). The fading of the interaction in $\mathbf{5m}^+$ was attributed to a quantum interference effect, i.e., a cancellation of the contributions of the two-electron transfer paths.

An electrochemical study on a series of *orto*- (**6o**), *meta*- (**6m**) and *para*- (**6p**) bis(ferrocenyl)ethynylbenzenes was carried out by Astruc[29] in order to get insight into the electrostatic or resonant nature of the interaction between ferrocenyl groups.

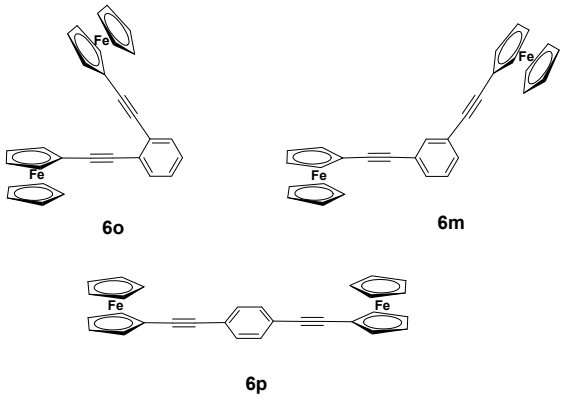

Previously, 1-bromo-3,5-bis(ferrocenylethynyl)benzene was reported by the Long and Zanello[30], for which only one oxidation wave was observed by CV accounting for a lack of electronic communication between the redox centres. Other poly(ferrocenyl) complexes resulted in the observation of a single wave in CV using nBu$_4$NPF$_6$ as the supporting electrolyte.[31]

Weakly coordinating anions with highly delocalized negative charge, such as $B(C_6F_5)_4^-$, allow minimization of nucleophilic attack on the radical cations. In addition, they undergo much weaker ion pairing than the traditional anions in low-polarity solvents. These properties make it possible to manipulate the anodic ΔE values, and the largest values are obtained in less polar solvents with low donor number.[22a]

CVs of **6m** of **6p** showed a single two-electron wave with nBu$_4$NPF$_6$ or nBu$_4$NB(C$_6$F$_5$)$_4$ as the supporting electrolyte, a result attributed to the absence of both electronic and electrostatic interaction. The *ortho* isomers **6o** showed a single two-electron wave using nBu$_4$NPF$_6$ due to the lack of significant electronic communication between the two ferrocenyl redox centres. However, wave splitting is observed for **6o** with nBu$_4$NB(C$_6$F$_5$)$_4$, which was ascribed to the presence of significant electrostatic repulsion between the two "naked" cationic centres in $\mathbf{6o}^{2+}$.

There is evidence that traditional anions such as BF_4^- and PF_6^- may react as nucleophiles with radical cations.[22a] Astruc suggested that the ΔE corresponds approximately to the electronic communication in the absence of other significant factor if a splitting between two CV waves of two equivalent redox centres is observed.[29a] However, it must keep in mind that an undetectable or small ΔE is not diagnostic of a negligible communication, since even in the case where a single electrochemical wave is observed a significant amount of mixed-valence species may be present in solution.[32] The values of K_c and ΔE determined by electrochemical measurements have been widely used for assessing the degree of electronic coupling in mixed-valence complexes. However, the electronic-coupling parameters derived from classical and semiclassical theoretical models[12a,b, 14b, 25] and from electrochemical studies are frequently in poor agreement.[22] Caution is needed in the interpretation of electrochemical data due to the considerable dependence of redox potential and reversibility on the nature of the solvent and supporting electrolyte.

Much better results and agreement with the theoretical treatment are usually provided by optical investigations in the NIR region where mixed-valence species typically absorb.

Indeed, we have recently synthesized the bis(ferrocenyl) complexes of *s*- and *as*-indacenes, **7a** and **7b**,[33] demonstrating that the rigid and planar indacene platform bonded to two terminal redox groups displays a redox chemistry that can be switched from a single two-electron transfer, using nBu$_4$NPF$_6$ as the supporting electrolyte, to two successive one-electron transfers with nBu$_4$NB(C$_6$F$_5$)$_4$.

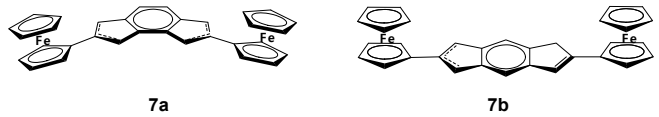

Despite the small ΔE values even in the presence of nBu$_4$NB(C$_6$F$_5$)$_4$, resolved by square wave voltammetry (Fig. 3), generation by chemical oxidation of the mixed-valence diiron cations and their characterization by optical spectroscopy were accomplished. Hush analysis of the IVCT bands in the NIR region indicated that $\mathbf{7a}^+$ and $\mathbf{7b}^+$ are Class II, moderate coupled, mixed-valence systems.

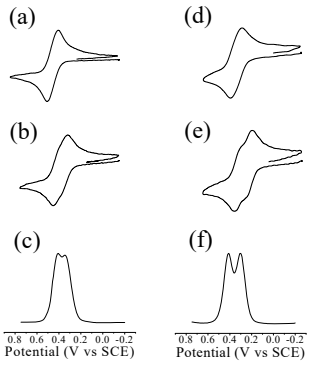

Fig. 3. Oxidative CVs in dichloromethane at 20 °C of **7a** with (a) 0.1 M nBu$_4$NPF$_6$, (b) 0.1 M nBu$_4$NB(C$_6$F$_5$)$_4$, (c) DPV with 0.1 M nBu$_4$NB(C$_6$F$_5$)$_4$. Oxidative CVs in dichloromethane of **7b** with (d) 0.1 M nBu$_4$NPF$_6$, (e) 0.1 M nBu$_4$NB(C$_6$F$_5$), (f) DPV with 0.1 M nBu$_4$NB(C$_6$F$_5$).

Moreover, ΔE separation was sensitive to the geometry of the organic bridge. In particular, as a result of higher ΔE separation, $\mathbf{7b}^+$ could be selectively produced in solution. The molar absorption coefficient of its IVCT band was higher than that of $\mathbf{7a}^+$, suggesting that the linear "*para*-like" *s*-indacene is a more efficient bridging ligand than the non-linear *as*-indacene in transmitting charge from the ferrocene to the ferrocenium terminal groups. Similarly, as previously reported by Coudret and Launay,[34] a single wave was observed for the bis(ferrocenyl)anthracene complex **8** and its TCNE

adduct **9** at the same potentials, corresponding to two close monoelectronic processes.

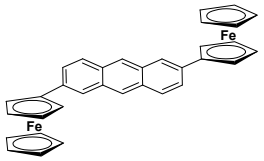

8

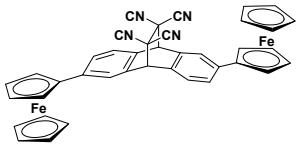

9

DPV allowed the resolution of the two processes and the determination of the ΔE and K_c values for **8** (72 mV and 17, respectively). The mixed-valence cations $\mathbf{8}^+$ and $\mathbf{9}^+$ were generated by controlled potential electrolysis and the obtained spectra in the NIR region showed intervalence transitions as broad bands. The resulting values of the electronic coupling parameters H were 260 cm^{-1} for $\mathbf{8}^+$ and 150 cm^{-1} for $\mathbf{9}^+$, indicating significant electronic interaction for both the mixed-valence species. Interestingly, in the latter, H decreases but did not vanish despite the loss of conjugated character.

In its early works,[35] Rausch described the synthesis of a series of compounds where up to four ferrocenyl groups are introduced on the cyclobutadiene ring of (η^4-cyclobutadiene)(η^5-cyclopentadieny1)Co, among which the two bis(ferrocenyl) isomers *cis*-CpCo($Fc_2Ph_2C_4$) (**10a**) and *trans*-CpCo($Fc_2Ph_2C_4$) (**10b**) were examined with the aim to inspect the effect of positional isomerism on the properties of the mixed-valence species $\mathbf{10a}^+$and $\mathbf{10b}^+$.

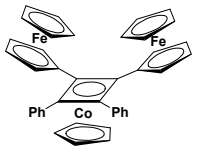

10a

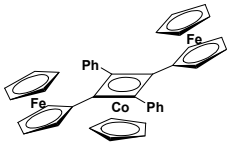

10b

Within CV experiments in dichloromethane containing nBu$_4$NPF$_6$ as the supporting electrolyte, both ferrocenyl groups of **10a** and **10b** isomers underwent two successive reversible oxidations at almost identical potentials separated by 190 and 170 mV, respectively.

Surprisingly, both mono and dioxidized forms of the two isomers gave rise to a band in the NIR region ($\mathbf{10a}^+$, $\tilde{\nu}_{max}$ = 8000 cm^{-1}; $\mathbf{10a}^{2+}$, 8930; $\mathbf{10b}^+$, 6950; $\mathbf{10b}^{2+}$, 9260) characterized by position, intensity, bandwidth, and solvent dependence typical of IVCT bands of class II mixed-valence species. Since an iron–iron coupling is not possible in the dications, the authors proposed that the intervalence transition arose predominantly from a Co(I)-Fe(III) coupling. This hypothesis was corroborated by the observation that the cation of the monoferrocenyl CpCo($FcPh_3C_4$) exhibited a band in NIR region ($\tilde{\nu}_{max}$ = 7840 cm^{-1}) similar to those seen for $\mathbf{10a}^{+/2+}$and $\mathbf{10b}^{+/2+}$.

Burrell and Officier[36] reported synthesis, structure and properties of bis(ferrocenyl)porphyrins, the α,α-5,15-bis(ferrocenyl)-2,8, 12,18-tetrabutyl-3,7,13,17-tetramethylporphyrin **11** and its nickel derivative **Ni-11**, for which a strong coupling between the two remote ferrocenyl moieties resulted upon single electron oxidation.

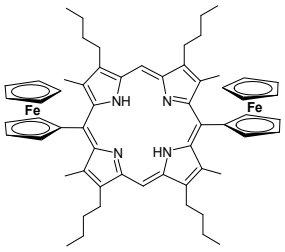

11

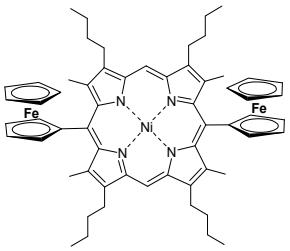

Ni-11

The CV of **11** and Ni-**11** showed two successive ferrocene-based oxidation waves separated by 190 and 410 mV, respectively. The large values of K_c calculated from the separation of the voltammetric waves, 1.6×10^3 for **11** and 8.5×10^6 for **Ni-11**, were consistent with the appearance, upon one electron oxidation, of low energy IVCT absorptions (at 1080 and 946 nm, respectively). The comparison of the small bandwidth $\Delta\tilde{\nu}_{1/2}$ = 1400 cm^{-1} for $\mathbf{Ni\text{-}11}^+$ with the value calculated by mean of eq. 8 (4900 cm^{-1}) indicates that this cation is a class III (highly delocalized) mixed-valence species. For $\mathbf{11}^+$, the experimental value $\Delta\tilde{\nu}_{1/2}$ = 2600 cm^{-1}, compared to the calculated value (4600 cm^{-1}), suggests a borderline class II/III behaviour. Accordingly to the trend of the electrochemical ΔE splitting, the nichel coordination strongly enhanced the magnitude of the iron–iron coupling. Similar effect was found by the metal-free and nichel-coordinated R,R-5,15-bis(ferrocenyl)-2,8,12,18-tetrabutyl-3,7, 13,17-tetraethylporphyrin.[37]

The metal–metal interaction in both **11** and **Ni-11**, at a separation more than 10 Å, is remarkably high and quite unexpected if considering that the related 5,10,15,20-tetraferrocenylporphyrin and 5,15-diferrocenyl-10,20-di-*p*-tolylporphyrin[38] display no such coupling.

A DFT calculation suggested that this strong coupling should be the result of extensive mixing of both ferrocenyl molecular orbital systems with that of the porphyrinic π-system. The low symmetry (≈ C_{2v}) of **11** and **Ni-11**, the possibility of extensive vibronic coupling owed to the restricted rotational flexibility of the ferrocenyl groups and transmitted into the porphyrin core, and the molecular dipole created by the α,α-porphyrin are the possible factors that may rationalize the strong coupling.

In order to understand how the ferrocenyl substituents located at specific *meso* positions in bis(ferrocenyl)porphyrins can influence long-range metal-metal coupling, two structural isomers of *meso*-substituted (bis)ferrocenyl-dipentafluorophenyl porphyrins, the "*trans*" with the ferrocenyl groups in the 5,15 positions, **12**, and the "*cis*" with the ferrocenyl groups in the 5,10 positions, **13**, were prepared and characterized by Swart.[39]

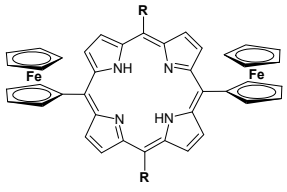

12, R = C_6F_5
14, R = C_6H_5

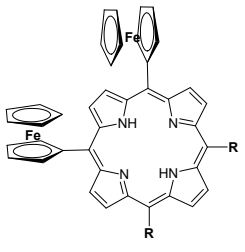

13, R = C_6F_5
15, R = C_6H_5

While CV experiment of **12** in the coordinating acetonitrile, using the traditional nBu$_4$NPF$_6$ supporting electrolyte, resulted in the overlapping of two oxidation waves, the CV and SWV experiments, conducted in dichloromethane in the presence of the low ion-pairing nBu$_4$NB(C$_6$F$_5$)$_4$ as supporting electrolyte, displayed two resolved waves but no significant differences between the first and second ferrocene-centred oxidations of two isomer isomers (111 mV for **12** and 115 mV for **13**) were found. The observed splitting with nBu$_4$NB(C$_6$F$_5$)$_4$ was mainly attributed to the presence of significant electrostatic repulsion between the two nonion-pairing cationic centres in the dication. However, since the optical properties of the **12**$^+$ and **13**$^+$ were not reported, the nature of the electronic coupling of these cations was not clarified.

In this context, addressing the question if the π system of the porphyrin is an efficient platform for electron transfer between ferrocenyl, Nemykin and Galloni[40] prepared and characterized the "*trans*" 5,15-bis(ferrocenyl)-10,20-diphenyl (**14**) and the "*cis*" 5,10-bis(ferrocenyl)-15,20-diphenyl (**15**).

The electrochemical removal of individual electrons from the ferrocene substituents indicated the existence of long-distance metal-metal interaction in both *cis* and *trans* isomers, a result supported by spectroelectrochemical and chemical oxidation experiments. Within CV experiments, the first oxidation of *trans* **14** occurred at lower potential then that of *cis* **15** and the ΔE separation between the two ferrocenyl-based oxidation wave of **14** and **15** were 208 mV and 150 mV, respectively. The related comproportionation constants are large enough to form stable mixed-valence species.

The analysis of the IVCT bands observed in the NIR region found for the mixed-valence cations **14**$^+$ and **15**$^+$ ($\tilde{\nu}_{max}$ = 11700, 11000 cm^{-1}, ε_{max} = 9300, 6100 M^{-1} cm^{-1} and $\Delta\tilde{\nu}_{1/2}$ = 2900, 4100, respectively) and formed under spectroelectrochemical and chemical oxidation conditions, suggested the existence of electron localization and class II behaviour in the Robin-Day classification. The values of the parameter H determined for **14**$^+$ and **15**$^+$ (910 and 1100 cm^{-1}, respectively), using the DFT calculated iron–iron distances as r in eq. 6, suggested somewhat higher metal electronic coupling in the *cis* isomer.

However, when the electronic coupling is pronounced, the true electron transfer distance r can be considerably shorter than the geometric distance r_g. Indeed, we note that the narrowness of the bands highlighted by comparing the experimental and calculated (eq. 8) half-bandwidths $\Delta\tilde{\nu}_{1/2}$ was more pronounced for the *trans* **14**$^+$. The value of the parameter Γ (eq. 9) found for **14**$^+$ (0.44) results higher than that of **15**$^+$ (0.19) clearly suggesting, to our opinion, that the *trans* disposition of the ferrocenyl groups significantly increases the strength of the metal–metal interaction with respect to that of the *cis* configuration. In addition, the observation that the molar absorption coefficient of the IVCT band of **14**$^+$ is higher than that of **15**$^+$ supports the proposition that the *trans*-substituted porphyrin is a more efficient bridging ligand than the *cis* in transferring the electron from the ferrocene to the ferrocenium groups. This conclusion was confirmed by Bucher for the *cis* 5,10-bis[1′-[2-(1,3-dithiolanyl)]ferrocenyl]-15,20-di(p-tolyl)porphyrin and *trans* 5,15-bis[1′-[2-(1,3-dithiolanyl)]ferrocenyl]-10,20-bi(*p*-tolyl)porphyrin,[41] although based only on the value of the voltammetric ΔE splitting.

In a series of papers[42] recently reviewed by the same author,[43] Lang described an elegant method allowing the calculation of the effective electron transfer distance within a specific series of molecules and of the different contributions to ΔG_c (= $-F\Delta E$) given by the statistical distribution $(RT/F)\times\ln(1/4))$, the electrostatic interaction (ΔG_e), the inductive factor (ΔG_i), and the resonance stabilization (ΔG_r).

A family of bis(ferrocenyl) five-membered heterocycles (**16**–**24**) were prepared and analysed.

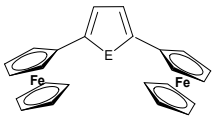

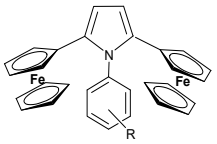

16, E = S
17, E = O
18, E= NMe
19, E= NPh

20, E = 4-NMe$_2$
21, E = 4-OMe
22, E = NMe
23, E = 3-F
24, E= 4-CO$_2$Et

Electrochemical CV and SWV measurements were carried out in dichloromethane in the presence of nBu$_4$NBPF$_6$ or nBu$_4$NB(C$_6$F$_5$)$_4$ as the supporting electrolyte. The use of dichloromethane and nBu$_4$NB(C$_6$F$_5$)$_4$ resulted in a better resolution due to the lower ion-pairing capabilities of B(C$_6$F$_5$)$_4^-$. Besides the higher quality of the electrochemical data for multiredox processes, the increase of wave splitting observed using the fluorinated electrolyte mostly reflects the electrostatic contribution to the stability of mixed-valence monocationic molecules. The enlargement of the wave separation is similar along the series **16**–**19** (130–140 mV).[31a, 42e, 44,] Therefore, taking into account that the iron–iron distances in this series are almost equal, electrostatic interactions should result similar. A comparison with analogous bis(ferrocenes) featuring 1H-phospholes bridges[45] revealed similar trends of the electrochemical properties, with the more easily oxidized complexes bearing the more electron donating heteroatoms, giving rise to larger ΔE values and accordingly higher stability of corresponding mixed-valence cations, in the sequence NPh (450 mV) > NMe (410 mV) > O (290 mV) ≈ PPh (280 mV) > S (260 mV).

It was found that the more electron rich the heterocyclic bridge was, the higher ΔE splitting appeared, an effect attributed to changes in the electron transfer properties of the connecting moiety. Assuming that the distances between the two ferrocenyl sites are similar along the series **16**–**24**, all the factors contributing to ΔG_c are constant with exception of the resonance stabilization ΔG_r:

$$\text{const} = RT\ln 1/4 + \Delta G_e + \Delta G_{in} \qquad (16)$$

For the cations **16**$^+$–**24**$^+$, the oscillator strength f [14a, 16] of the IVCT absorptions increases with the degree of intermetallic communication:

$$f = (4.6\times10^{-9})\varepsilon_{max}\Delta\tilde{\nu}_{1/2} \qquad (17)$$

The cations **16**$^+$–**24**$^+$ showed a linear relationship between ΔE and f as predicted by eq. 16 for a series of molecules with similar geometries and electrostatic properties. This relation could be described for the first time in organometallic chemistry and offers the possibility to estimate r which is difficult to obtain experimentally.

In fact, combination of eqs. 16 and 17 lead to a linear relationship between the oscillator strength f and ΔE (Fig. 3). From the slope, the effective electron transfer distance r was calculated (2.05 ± 0.05 Å), much shorter than the geometrical iron–iron distances, and used to determine H parameters according to Hush equation (eq. 6).

$$\frac{f}{4.6\times10^{-9}} = \frac{const\times r^2}{8.49\times10^{-4}} + \frac{F\times r^2}{8.49\times10^{-4}}\Delta E \qquad (18)$$

Finally, from the intercept and using eqs. 13 and 16, the contributions to ΔG_c, as the sum the electrostatic and the inductive factors (ΔG_e + ΔG_i) and the resonance stabilization (ΔG_r), were calculated.

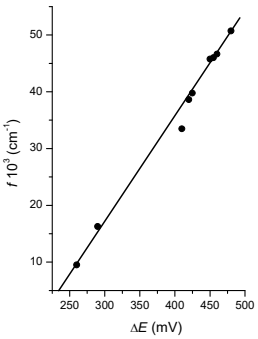

Fig. 3 Correlation of f and the ΔE values of **16**–**24** (R^2 = 0.987).

Barlow and O'Hare[46] synthesized a series of mixed bis(ferrocenyl) complexes in which two FeCp*Cp (Cp* = pentamethyl-cyclopentadienyl) are linked by the saturated bridges CMe_2, $SiMe_2$, $GeMe_2$ and Si_2Me_4. SWV of **25**–**27** showed that the ΔE separation between the oxidation waves decreases for the bridging ligand in the order CMe_2 > $SiMe_2$ > $GeMe_2$, a result consistent with the increasing metal–metal distance with a through-space, essentially electrostatic effect which likely dominated the value of the related comproportionation constant K_c.

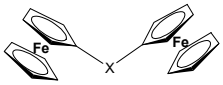

25, X = $C(Me)_2$
26, X = $Si(Me)_2$
27, X = $Ge(Me)_2$
28, X = Si_2Me_4

The electronic coupling was quantitatively probed by the analysis of the IVCT absorption in the NIR region of mixed-valence cation. The electronic coupling parameter H was determined by analysis of the IVCT band using Hush's relationship (eq. 6), and the cation **25**$^+$–**27**$^+$ were classified as Class II mixed-valence species. In a Class II system, the $\tilde{\nu}_{max}$ energy of the IVCT band represents the reorganisation energy λ for the intramolecular electron-transfer reaction. The value of $\tilde{\nu}_{max}$ slightly increases with the size of the bridging atom, likely due to differences in external reorganisation energy: as the metal–metal separation increases, the electron transfer distance will increase and consequently the solvent reorganisation parameter becomes larger.

The degree of electronic coupling decreases in the order CMe_2 > $SiMe_2$ > $GeMe_2$. This observation is unusual if compared with previous results on metallocenes linked by saturated bridges. In those studies, a stronger coupling through a Si-bridge was suggested,[10b, 47] due to conjugation through empty, low-lying σ* or d orbitals of Si, which may enable greater coupling.[48]

Differently, Barlow and O'Hare suggested that the decrease in the order CMe_2 > $SiMe_2$ > GeMe2 indicates that the coupling is predominantly through space in **25**$^+$–**27**$^+$. Assuming the same molecular conformation, the metal–metal separation should increase with the size of the bridging atom; hence, the distance parameter r in eq. 6 should increase and the value of H calculated for the $SiMe_2$ and $GeMe_2$ systems may be overestimated, reinforcing the observed trend. Moreover, the observation of a strong IVCT band for **28**$^+$ pointed out the importance of a strong through-space coupling.

We have recently reported the synthesis of a new series of 3_{10}-helical peptides of different length (**29-33**) containing two terminal ferrocenyl units and based on the strongly foldameric α-aminoisobutyric (Aib).[49]

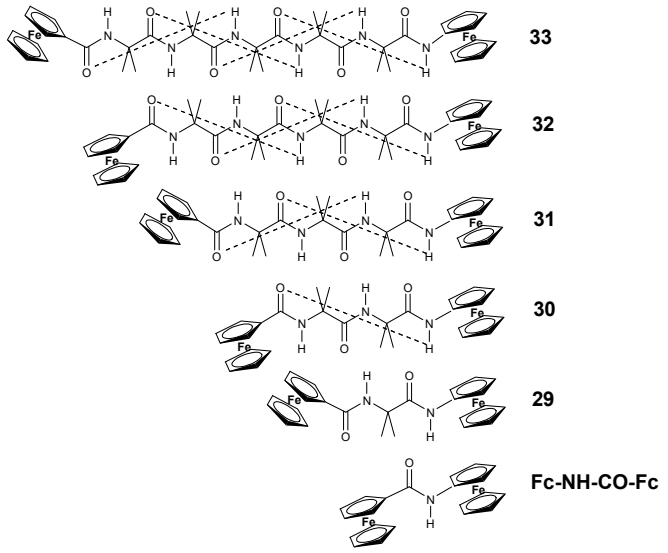

The intrinsic redox asymmetry of the C-terminal and N-terminal ferrocenyl groups permitted to generate, selectively, the cationic and dicationic derivatives. The end-to-end effects of electron holes generated by single and double oxidations were analysed by means of electrochemical and spectroelectrochemical techniques. The results indicated that charge transfer across the peptide occurs in the five peptides. In particular, in the pentapeptide (**33**), charge is transferred through an intramolecular iron–iron separation of 14 Å. The trends of the oxidation potentials, previously observed by us in the two series of monometallic ferrocenyl-peptides,[50] depend on the position of the ferrocenyl groups in the chain and on macrodipole orientation (Fig. 4).

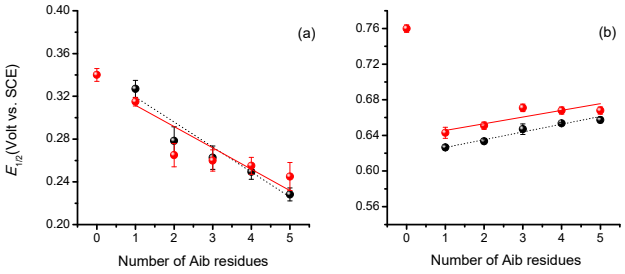

Fig. 4 $E_{1/2}$ oxidation potentials of FcNHCOFc and **29**–**33** (red circles), and of Z–$(Aib)_n$–NH–Fc (n = 1–5) (a, black circles) and Fc–CO-$(Aib)_n$–OMe (n = 1–5) (b, black circles) peptides, obtained by CV in dichloromethane containing 0.1 M nBu_4NPF_6 as the supporting electrolyte; Au disk electrode (d = 0.5 mm); scan rate 0.5 Vs^{-1}; T 20 °C.

Indeed, as the $(Aib)_n$ peptide grows, oxidation of the ferrocenyl occurs easier or harder depending on the orientation of the macrodipole moment of the peptide chain, that is away from the N-terminal Fc or towards the C-terminal ferrocenyl moiety, respectively. Since no IVCT band was observed, these effects can be ascribed to inductive and/or electrostatic interaction transmitted through the intramolecularly hydrogen-bonded networks.

The strongest effect is observed for tripeptide **31** in which two intramolecular C=O···H–N hydrogen bonds are formed, establishing a particularly efficient electron transfer shortcut.[51]

Metal-metal electron delocalization in linkage structures assembled via noncovalent are extremely rare. Kaifer[52] reported the preparation and properties of a ferrocene derivative containing a quadruple hydrogen bonding motif designed to self-recognize, forming a fascinating highly stable hydrogen-bonded dimer that contains two identical ferrocene centres separated by more than 10 Å (**34**).

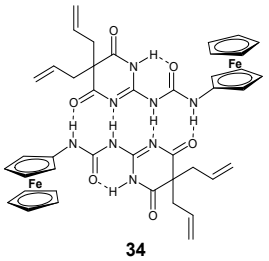

34

CV experiments with **34** in acetonitrile/nBu$_4$NPF$_6$ solution showed one reversible oxidation waves at 0.43 V vs Ag/AgCl, but enriching the solvent mixture in dichloromethane, a solvent less polar than acetonitrile, a second reversible oxidation waves at 0.82 V vs Ag/AgCl appeared. The stability of the mixed-valence dimer **34**$^+$ in dichloromethane solution allowed the detection of an IVCT band in the NIR spectral region at $\tilde{\nu}_{max}$ = 8370 cm^{-1}. Surprisingly, the spectral characteristics, in particular the experimental bandwidth ($\Delta\tilde{\nu}_{1/2}$ = 560 cm^{-1}) compared to the value predicted by Hush theory (eq. 6, $\Delta\tilde{\nu}_{1/2}$ = 4400 cm^{-1}), indicated that the extent of electronic coupling between the ferrocenyl moieties in the dimer is extremely strong and **34**$^+$ is a totally delocalized class III system with very high Γ parameter (0.87) in the Robin-Day and Brunschwig-Creutz-Sutin classifications. Remarkably, this is the first example, and to the best of our knowledge unique so far, of a noncovalent mixed-valence species, constituted by two identical halves assembled by four hydrogen bonds.

Applications in useful devices of compounds containing two or more connected ferrocenyl moieties, are often problematic mainly because electronic coupling between the two redox sites rapidly decreases with metal-metal distance. A combination of factors influences the communication between the connected ferrocene moieties, including the type of connection, the length of the connector and the orientation of the two ferrocenes.

Among the molecules which are excellent benchmarks for testing the paradigm of quantum cellular automata (QCA), which is based on field-coupled charge containers,[53] a symmetric mixed-valence complex is the simplest building block for a QCA cell. The binary states (the Boolean states) are obtained by changing the position of an electron from one metal centre to the other. Bis(ferrocenyl) mixed-valence complexes joins the family of molecular electronics[54] in the QCA paradigm and found a successful application with 3,6-bis(1-ethylferrocen)-9H-carbazol-9-yl-6-hexan-1-thiol (**35**) and its enantiomers.[55]

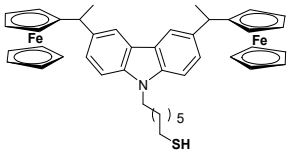

35

In a QCA, the interplay between electronic coupling and electrostatic interaction is a crucial point: quantum dots are arranged in functional cells connected by tunneling pathways, each containing two mobile charges which tend to localize on opposite corners due to electrostatic repulsion, encoding the Boolean states 1 and 0 (fig. 5). The adjacent cells interact electrostatically and their ground state configuration depends on the reciprocal charge positioning in the cells. In fig. 5, the cell includes also two middle dots corresponding to a different ground state, imposed by an external electric field (the clock) which allows directional information flow.[56]

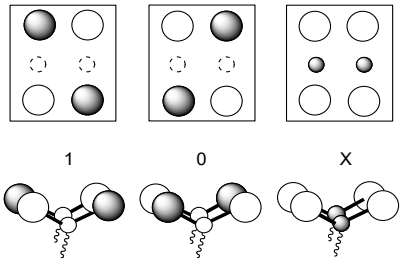

Fig. 5 The three Boolean states of a six-dot cell: 1, 0 and one null (X), depending on the charges localization (gray shading). The middle dots (dashed) have different ground-state energy: the null state is forced upon application of the clocking electric field. The cell is implemented by two paired molecules, each including three ‘‘quantum-dot’’ moieties such as **35**.

Complex **35** addressed all the three requisites which are functionally demanded by QCA operation: (i) defined Boolean states were granted and readable, as the weak conjugation found between ferrocenyl groups favoured neat charge localization, keeping the Boolean states well distinct; (ii) the geometry of dots, which strongly affects electrostatic interaction, was stable after solid state immobilization; (iii) applying a proper clocking electric field could delete the previously stored state.

At room temperature and low scan rate (1 V s^{-1}), the CV of **35** in THF and nBu$_4$NPF$_6$ as the supporting electrolyte displayed one reversible two-electron oxidation peak at $E_{1/2}$ = 0.35 V associated with the reversible oxidation of the two equivalent ferrocenyl moieties. However, the two-electron peak is split into two reversible one-electron peaks at high scan rate (10 V s^{-1}). The same effect were obtained at low temperature (218 K) and lower scan rate (1 V s^{-1}). At more positive potentials **35** underwent a further reversible oxidation process with $E_{1/2}$ = 1.25 V associated with the reversible oxidation of the carbazole unit.

These results indicated the existence of weak through bond interaction between the ferrocenyl units allowing a description of **35**$^+$ in terms of the localized redox sites. The observed weak conjugation favours neat charge localization keeping the Boolean states well distinct. Moreover, solid-state electrochemistry of mixed self-assembled monolayers (SAMs) of **35** and hexane-1,6-dithiols demonstrated the effective immobilization and stability of **35** on the surface and excluded undesired structural rearrangements upon application of the electric field. Finally, functionality simulation

showed that charge localization on the carbazole can be obtained by clocking field values in the order of a few V nm^{-1}, so encoding a neutral state as required for correct QCA operation.

Tris(ferrocenyl) complexes

Investigations on three families of tris(ferrocenyl) systems[57], namely "star-shaped", linear and cyclic, should provide a mean of bridging the gap between the interpretation of the electron-transfer process in simple bimetallic molecules and that in multi-component systems.

Homoleptic tris(ferrocenyl) "star-shaped" derivatives of B, N, P, Sb, Bi have been prepared and characterized so far (**36**-**40**).[58] In addition, tris(ferrocenyl) compounds of PO (**41**), C (**42**)[59] and Si (**43**)[60] were also synthesized.

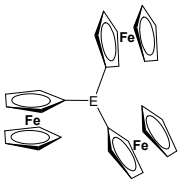

36, E = B
37, E = N
38, E = P
39, E = Sb
40, E = Bi
41, E = PO
42, E = CH
43, E = SiH

The charge transfer properties of a limited number of these molecules were investigated and those exhibiting electron transfer transition include the mixed-valence cations of tris(ferrocenyl)phosphine oxide (**41**) and tris(ferrocenyl)methane (**42**). For $\mathbf{42}^{+}$, the electronic coupling H = 205 cm^{-1}, estimated using the Hush relationship (eq. 6), is consistent with a mixed weakly coupled class II system.[59]

Monoxidized tris(ferrocenyl)borane (**36**) and tris(ferrocenyl)phosphine (**38**) did not exhibit the NIR transition. The IVCT band found for the σ-bond bridged derivative **42** was attributed to a through-space mechanism. Conversely, it was suggested that the presence of the transition in the phosphine oxide **41**, absent in the phosphine derivative, may be due to a difference in the dp-π overlap of phosphorus and the cyclopentadienyl rings in the two systems. [59]

Tris(ferrocenyl)amine (**37**) showed three well-resolved reversible oxidation waves within CV experiments in acetonitrile with $NaClO_4$.[61] This is an unusual molecule, as shown by its molecular structure,[62] since it contains three ferrocenyl groups surrounding an almost planar nitrogen atom. In addition, the short C(ring)-N bonds (average 1.414 Å) indicate partial double-bond character between the nitrogen and the cyclopentadienyl ring suggesting the existence of a strong electronic interaction between the amine nitrogen and the ferrocenyl substituents, resulting in resonance interaction as an important factor in the stabilization of the ferrocenium by nitrogen.

CV of triferrocenylsilane (**43**) displayed three reversible oxidation waves in dichloromethane solutions containing either PF_6^- or $B(C_6F_5)_4^-$ electrolyte anions, closely spaced with nBu$_4$NPF$_6$ and well-separated with nBu$_4$NB(C$_6$F$_5$)$_4$, indicating a good interaction between the ferrocenyl moieties.[60] Applying to these results what suggested by Astruc,[29] when nBu$_4$NPF$_6$ is used as the supporting electrolyte in dichloromethane, the strong ion pairing between PF_6^- and the cationic substrates leaves very little electrostatic effect. The observed splitting between the subsequent CV waves of the equivalent ferrocenyl groups should roughly correspond to electronic interaction in the absence of other significant factors, possibly with a through-space mechanism. The increased wave separation in the presence of nBu$_4$NB(C$_6$F$_5$)$_4$ is reasonably due to electrostatic interaction.

Recently, Lang[63] presented the synthesis, electrochemical and spectroelectrochemical behaviour, and DFT calculations of "star-shaped" tris(ferrocenyl) substituted six-membered (hetero)aromatic benzene (**44**), pyridine (**45**), and triazine (**46**).

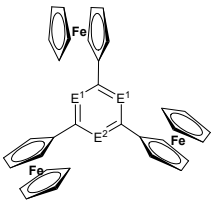

44, $E^1 = E^2$ = CH
45, E^1 = CH, = E^1 = N
46, $E^2 = E^1$ = N

In contrast to the electrochemical investigation of **44** using nBu$_4$NClO$_4$ as supporting electrolyte in benzonitrile, resulting in a simultaneous oxidation of the three ferrocenyl substituents,[31a] the use of nBu$_4$NB(C$_6$F$_5$)$_4$ allowed the separation of the redox events. Similarly, the tris(ferrocenyl)-substituted molecules **45** and **46** showed three well-defined and separated reversible one-electron redox processes. According to the ΔE values, the thermodynamic stability of the mixed-valence species, determined by the comproportionation constant K_c, increased in the order **46** > **45** > **44**. Concerning the nonresonance terms of ΔG_c, the increase of ΔE splitting and K_c was attributed to the stabilization of the charge by delocalization into the aromatic ligand.

For the mixed-valence species $\mathbf{44}^{n+}$, and $\mathbf{45}^{n+}$ (n = 1, 2) broad and low-energy absorptions between 10000 and 4000 cm^{-1} with different intensities were observed. These IVCT transitions are indicative of electronic interactions between the Fe(II)/Fe(III) iron centres along the benzene and pyridine bridges. Their spectroscopic characteristics allowed assigning the mixed-valence to very weak coupled class II systems. Interestingly, the absence of ΔE splitting for **44** with nBu$_4$NClO$_4$ as supporting electrolyte was not symptomatic of lack of electronic coupling.

No absorption in the NIR region appeared by oxidation of **46**, allowing the classification of this compound as a class I system. Thus, the observed ΔE splitting was attributed to electrostatic interactions between the positively charged ferrocenyl groups in $\mathbf{37}^{2+}$ and $\mathbf{46}^{3+}$, and the highest ΔE values found for **46** were ascribed to the nonresonance terms of ΔG_c.

These results prompt to conclude that systems with similar architecture and splitting between consecutive redox waves may still differ with respect to the nature and strength of the electronic interactions.

The CV of "star-shaped" 1,3,5-tris(ferrocenyl)ethynybenzene complex **47** reported by Astruc[29] showed a simultaneous oxidation of the three ferrocenyl substituents with nBu$_4$NPF$_6$ as the supporting electrolyte, attributed to the absence of electronic communication, and three well-separated redox events with nBu$_4$NB(C$_6$F$_5$)$_4$.

However, for *meta*-bis(ferrocenyl)ethynylbenzene (**6m**) as well as for the 1,3-bis(ferrocenylethynyl)arene complexes containing bromo **(48)**, ethynyl **(49)**, trimethylsilyethynyl **(50)** and pentamethylferrocenylethynyl **(51)** substituents in the third *meta*

position, only a single wave was observed for the two ferrocenyl group even with nBu$_4$NB(C$_6$F$_5$)$_4$.

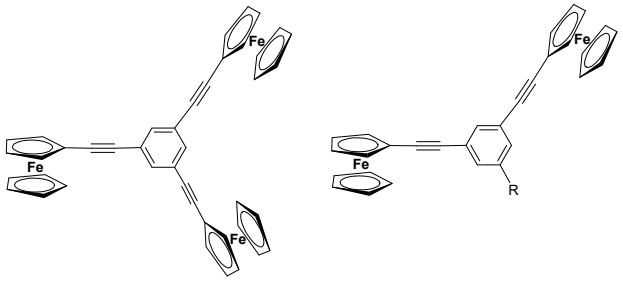

47

48, R = Br
49, R = C_2H
50, R = C_2SiMe_3
51, R = C_5Me_5FeCp

In these compounds, in order to minimize the electrostatic repulsion, the two oxidized ferrocenyl groups were supposed to lie at opposite sides respect to the plane of the benzene ring. When a third ferrocenyl group is present in *meta* position, there is "frustration",[64] meaning that the third ferrocenyl must lie at an intermediate position enhancing the electrostatic effect among the three positively charged sites and causing the splitting of the three ferrocenyl CV waves. In the case of **51**, the charge of pentamethylated ferrocenyl is partially shielded causing the decrease of the electrostatic interaction with the two other oxidized ferrocenyl that arrange at opposite sides in order to minimize their mutual repulsion.

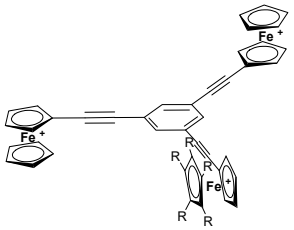

"Frustration" in **47**$^{3+}$ and **51**$^{3+}$
R = H, Me

We have recently described the synthesis, electrochemistry of a family of mono- (**52**), bis- (**53**) and tris(ferrocenyl) (**54**) complexes of dihydro-1H-trindene (TdH),[65] a polycyclic hydrocarbon synthesized by Katz and Ślusarek in the early 1980s.[66] The use of TdH as a metal bridging ligand is particularly favourable because strain is minimal as a consequence of the presence of only five- and six-membered rings.

Complex **54** is a "star-shaped" tris(ferrocenyl) system structurally related to the diferrocenyl complex **7a** previously investigated by us. Within CV and SQV experiments (Fig. 6), the bimetallic **53** and trimetallic **54** complexes display a redox chemistry that could be switched from a single to two consecutive oxidation processes by changing the supporting electrolyte from nBu$_4$NPF$_6$ to nBu$_4$NB(C$_6$F$_5$)$_4$.

By simple variation of the counter-ion of the supporting electrolyte PF_6^- with the weak nucleophilic and ion-pairing $B(C_6F_5)_4^-$ anion, the unresolved two-electron oxidation wave of **53** is split into two consecutive one-electron oxidation waves. Similarly, the three-electron oxidation waves of **54** are partially resolved in two consecutive one-electron and two near simultaneously occurring one-electron oxidations oxidation waves.

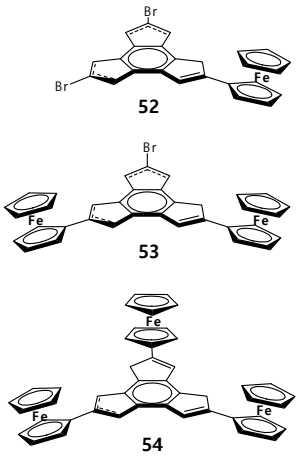

52

53

54

As a result of the ΔE splitting, **53**$^+$ and **54**$^+$ can be selectively produced in solution.

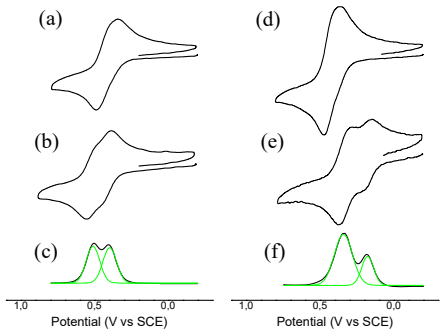

Fig. 6 Oxidative CVs in dichloromethane , scan rate v = 0.5 V s^{-1}, of **53** with (a) 0.1 M nBu$_4$NPF$_6$, (b) 0.1 M nBu$_4$NB(C$_6$F$_5$)$_4$, (c) SWV with 0.1 M nBu$_4$NB(C$_6$F$_5$)$_4$. Oxidative CVs in dichloromethane of **54** with (d) 0.1 M nBu$_4$NPF$_6$, (e) 0.1 M [nBu$_4$NB(C$_6$F$_5$)$_4$. (f) SWV with 0.1 M nBu$_4$NB(C$_6$F$_5$)$_4$.

Hush analysis of the IVCT bands in the NIR region clearly indicated that **53**$^+$ and **54**$^+$ are class II mixed-valence systems. The narrowness of these bands was highlighted by comparing of the experimental and calculated half-bandwidths. Remarkably, the value of Γ found for the trimetallic **54**$^+$ species is higher than that of bimetallic **53**$^+$, which clearly suggests that the presence of the third ferrocenyl group in **54**$^+$ significantly increases the strength of the metal-metal interaction with respect to that of the structurally related diferrocenyl cation **53**$^+$. Significantly, as found for **7**, **8** and **44**, the absence of ΔE splitting with ion-pairing or nucleophylic supporting electrolytes was not indicative of lack of electronic coupling.

Pertaining to linear multi(ferrocenyl) systems, in one of its early works Meyer[67] reported the oxidation state and electron-transfer properties of linked 1,1'-triferrocene (**55**), 1,1'-tetraferrocene (**56**) compared with those of the parent biferrocene.

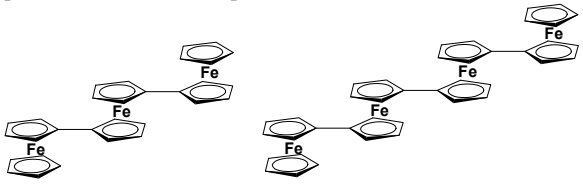

55 **56**

The CV displayed a number of reversible waves equal to the number of ferrocenyl groups in the oligomer complex. The pattern of the oxidation potentials accounted for the electron-donating properties of the ferrocenyl group, in the order biferrocene **>** **56** > **55**. Weakly electronic coupling was measured between Fe(II) and Fe(III) sites for the mixed-valence ions of **55**$^{+}$, **55**$^{2+}$ and **56**$^{2+}$.

In particular, the IVCT energy of the mixed-valence cation **55**$^{+}$ detected in the NIR region ($\tilde{\nu}_{max}$ =5590 cm^{-1}, ε_{max} = 1720 M^{-1} cm^{-1}) was similar to that found for (Fc–Fc)$^{+}$ ($\tilde{\nu}_{max}$ =5260 cm^{-1}, ε_{max} = 760 M^{-1} cm^{-1}), supporting valence localization (Class II) for the trinuclear system. The presence of two donor Fe^{II} centres and one acceptor Fe^{III} centre is responsible of the intensity enhancement of a factor of two in the IVCT band of **55**$^{+}$ over the (Fc–Fc)$^{+}$ case.

Even if the central ferrocenyl unit is reasonably the first centre to be oxidized, as it bears two electron-donating substituents, reactants and products of electron transfer in **55**$^{+}$ are almost energetically equivalent, being the energy difference between (Fc–Fc^{+}–Fc) and (Fc^{+}–Fc–Fc) with the former slightly favoured by the ferrocenyl substituent effects (≈ 30 mV) and the latter by a statistical factor of 2 (≈ 18 mV). The IVCT molar absorption coefficient of **55**$^{+}$ was much higher than that of (Fc–Fc)$^{+}$. This enhancement, typical of these 1,1'-oligoferrocene, was explained by considering the existence for **55**$^{+}$ of two equivalent transitions, that are Fc–Fc^{+}–Fc → Fc^{+}–Fc–Fc and Fc–Fc^{+}–Fc → Fc–Fc–Fc^{+}.

Nishihara[68] reported an electrochemical and optical investigation on a series of (1,1'-dihexylferrocene-1,1'-diyl) oligomers from bis to hexa(ferrocenyl) (**57**–**61**).

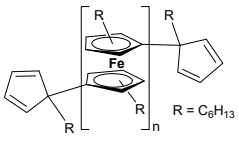

57, n = 2
58, n = 3
59, n = 4
60, n = 5
61, n = 6

Their redox potentials, regarding all the steps of one-electron transfer, were determined and the IVCT bands for the mixed-valence states were analysed.

The bandwidths of the intervalence transitions were comparable to those calculated from Hush theory and consistent with a localized Class II classification. Interestingly, it was observed a shift of $\tilde{\nu}_{max}$ to higher energy and a decrease of ε_{max} as the oxidation number for each oligomer increases, an effect more marked for even-numbered oligomers, and a shift to lower energy of $\tilde{\nu}_{max}$ for the monocationic forms of the oligomers as the number of ferrocene units increases.

The shift of $\tilde{\nu}_{max}$ was rationalized by taking into account the change in "neighboring-site combination" by photoelectron transfer, assuming that the mixed-valence states are linear combination of unoxidized (Red) and oxidized (Ox) ferrocenyl groups. Red-Ox combination is attractive while the Ox-Ox combination is repulsive. In the case of the cation of bis(ferrocenyl) **57**$^{+}$, the optical transition of Red−Ox yields Ox−Red and no adjustment in the iron−iron distance is required during the relaxation process. Conversely, for the cation of tris(ferrocenyl) **58**$^{+}$, the transition from Red−Ox−Red to Ox−Red−Red should involve a modification of the internuclear distance and requires more energy than Red−Ox to Ox−Red transition in **57**$^{+}$, not only for the energetic difference between different ground states but also for the tension resulting from the difference in iron−iron distances between Red−Ox, Red−Red and Ox−Ox combinations. The Red–Ox distance is the shortest due to the attractive interaction by the electronic delocalization and the Ox–Ox distance is the longest due to the electrostatic repulsion.[69]

Similar shifts to higher energy of the IVCT band with increasing oxidation state were found in a series of linear oligo(ferrocenyldimethylsilanes) from two to nine ferrocenyl units prepared by Gieger (**62**–**69**).[70]

Their ΔE splittings were not large enough to generate selectively the single mixed-valence states, due to weaker metal−metal interaction through the dimethylsilylene moiety. For oligomer systems containing an odd number of ferrocenyl groups, two reversible redox waves of varying intensities were observed, suggesting that two unresolved one-electron processes were present. For the tris(ferrocenyl) **63** and the other systems with an even number of iron centres larger than two, three reversible redox processes of varying intensities were found.

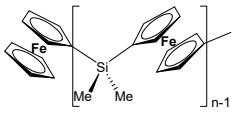

62, n = 2
63, n = 3
64, n = 4
65, n = 5
66, n = 6
67, n = 7
68, n = 8
69, n = 9

As the chain length of both odd and even oligomers increased, only two reversible redox processes could be observed: alternating ferrocenyl sites are first oxidized, a situation which minimizes the electrostatic repulsion, and the iron sites in-between are oxidized at a higher potential. An X-ray diffraction study of tris(ferrocenyl) **63**$^{2+}$ supported this hypothesis.

Spectroelectrochemical experiments for partially oxidized oligo(ferrocenylsilanes) showed weak IVCT absorptions ($\tilde{\nu}_{max}$ = 7500–9000 nm cm^{-1}, ε_{max} ≤ 150 M^{-1} cm^{-1}) typical of class II mixed-valence species. The trinuclear **63**$^{+}$ and binuclear **62**$^{+}$ monocation displayed IVCT characteristics similar in energy, extinction coefficient and half-heigth bandwith, resulting in a metal–metal coupling weaker than that of biferrocene.[71]

Very few electrochemical and spectroscopic studies have been reported on cyclic ferrocenyl triads in which rigid, two-dimensional C_3-arrays are defined by directly linking three cyclopentadienyl groups.

Bunz[72] reported the preparation of the first organometallic dehydroannulenes (**70** and **71**). These cyclic conjugated triferrocene compounds could be assembled by directly linking cyclopentadienyl groups through butadiyne linkers to define a rigid cyclic array.

The electrochemistry of **70** and **71** was investigated. While *anti* **70** displayed three sequential one-electron oxidation processes at 0.61, 0.74 and 0.83 V, indicative of the formation of detectable mixed-valence intermediates, *syn* **71** exhibited only two waves at 0.61 and 0.78 V, involving one and two electrons, respectively. The observed splittings are relatively small, suggesting that electronic and electrostatic interactions are weak in these systems. Interestingly, the first oxidation potentials are identical, while the ΔE splitting between the first and second waves are different, 0.23 and 0.17 V,

leading to the conclusion that, albeit the distance between ferrocenyl groups are relatively large, **70** and **71** display different electrochemical properties depending on the their geometry.

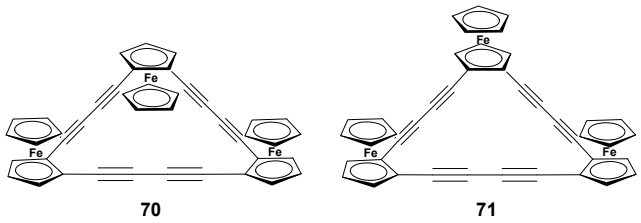

70 **71**

Unfortunately, the optical properties of the mixed-valence cations $\mathbf{70}^{+/2+}$ and $\mathbf{71}^{+/2+}$ were not reported.

We have recently reported the synthesis of the prototypical cyclic metallocene triads, namely the isomers *syn*,*syn*,*anti*-[(FeCp)$_3$Td] (**72**) and *syn*,*syn*,*syn*-[(FeCp)$_3$Td] (**73**) which can be figured out as the "fusion" of three ferrocenes into a rigid cyclic array.[73]

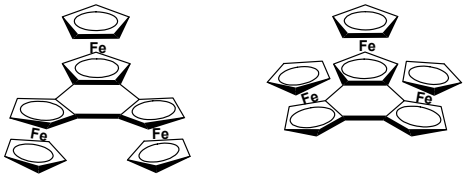

72 **73**

The CV oxidation of **72** in dichloromethane/nBu$_4$NPF$_6$ proceeded in three one-electron steps, the first and second fully reversible at $E_{1/2}$ = 0.23 and 0.61 V vs. SCE, the third chemically irreversible and nondiffusion-controlled (E_p = 0.94 V) with a typical stripping peak as its cathodic counterpart (Fig. 7).

The ΔE splitting between the first and second wave, as well as the related value of the comproportionation constant, is indicative of the thermodynamic stability of the cationic species $\mathbf{72}^+$ which could be generated by chemical oxidation and analysed at room temperature by optical spectroscopy.

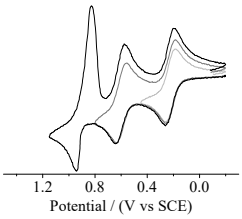

Fig. 7 CVs at different potential scan reversals of **72** in dichloromethane at Au disk electrode (d = 0.5 mm), scan rate v = 0.5 V s^{-1}, T = 20 °C.

Gaussian deconvolution of the spectrum obtained in the NIR/IR region showed three IVCT bands at 3430, 5310 and 7030 cm^{-1} (Fig. 8).

Considerable complexity may be expected in the theoretical analysis of IVCT transitions in trinuclear complexes due to the presence of multiple electronically coupled redox centres. As the electronic coupling increases to almost delocalized and delocalized, the classical Hush model is no longer suitable and trimetallic complexes have been shown to manifest properties that are different from those of their related bimetallic systems[10e] due to the possibility of itinerant "extra" electron hopping over the coupled sites.[74]

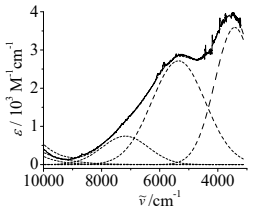

Fig. 8 NIR/IR spectrum of the $\mathbf{72}^+$ cation in dichloromethane (straight line) and Gaussian de-convolution (dashed lines).

More importantly, the influence of the third metal is such that within the three-site classical model the localized-to-delocalized transition is favoured relative to the two-site case,[12a,b] although this effect were not been experimentally verified before. [10e]

Remarkably, we provided rare experimental evidence that the introduction of a third metal centre increases the strength of the metal–metal interaction with respect to that of the structurally related binuclear systems.[75]

The IVCT bands of $\mathbf{72}^+$ appeared at low energy, narrow and solvent-independent, as expected for an almost delocalized Class II–III mixed-valence system. In contrast, Class II behaviour was observed for the structurally related cations of the bimetallic [(CpFe)$_2$(as-indacenediide)] isomers **74** and **75**, previously prepared by some of us. [75]

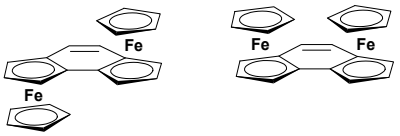

74 **75**

The Γ value (0.51–0.55 from eq. 9) obtained for the three bands supported the assignment of the mixed-valence $\mathbf{72}^+$ to the borderline Class II–III.

These results suggested that introduction of the third fused ferrocenes favours the localized-to-delocalized transition and are consistent with fast electron transfer and valence averaging on the NIR/IR timescale with no contribution of the solvent to the reorganization energy. As expected for a Class II–III regime, the solvent is averaged and the spin density, according to DFT calculations on $\mathbf{72}^+$, is localized.

The spectrum of $\mathbf{73}^+$ revealed a well-defined band at higher energy (10480 cm^{-1}) and lower intensity than that of isomer $\mathbf{72}^+$. The value of Γ = 0.31 were indicative of a weaker metal–metal electronic coupling when the three irons are in a *syn*,*syn*,*syn* configuration, but higher that that found for the structurally related bimetallic cation $\mathbf{75}^+$.

Tetra(ferrocenyl) complexes

Homoleptic tetra(ferrocenyl), EFc$_4$, derivatives of the Group 14 elements C, Si, Ge, Sn, and Pb have been prepared (**76**–**80**).[58]

SiFc$_4$ **77**[76] and Sn[(C$_5$H$_5$)(C$_5$H$_3$CH$_2$NMe$_2$)Fe]$_4$ **82**[77] have been prepared and fully characterized including investigation of electrochemical properties.

Cyclic voltammetry of **77** in benzonitrile showed four resolved and reversible oxidations waves with wave separations of 0.18, 0.14 and 0.10 V.

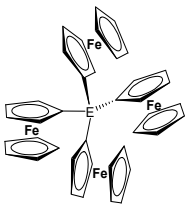

76, E = C
77, E = Si
78, E = Ge
79, E = Sn
80, E = Pb
81, E = B

The spread of the four potentials over 420 mV indicated appreciable interactions among the ferrocenyl groups upon successively oxidation. Instead, a solution of **82** in dichloromethane/nBu$_4$NPF$_6$ was oxidized in three steps with splitting of 0.12 and 0.14 V in a 2e/1e/1e sequence.

The zwitterion BFc$_4$ **81**,[78] provided four reversible one-electron oxidations with an even larger overall spread of 590 mV. Remarkably, **81**, which contains one iron(III) and three iron(II) units, has been characterized as a mixed-valence system in solution with a broad IVCT band at 4550 cm^{-1} and localized valencies in the solid state.[79]

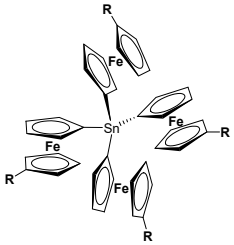

82, R = CH_2NMe_2
83, R = $COOCH_3$

Heinze[80] has isolated and fully characterized the substituted tetraferrocenylstannane Sn[($C_5H_4COOCH_3$)(C_5H_4)Fe]$_4$ (**83**) which was oxidized in three steps to the tetracation in a 1e/1e/2e sequence with a splitting of 0.12 V each, suggesting some interaction. The lack of coplanarity of the redox-active subunits in the congested EFc$_4$ compounds indicated that electronic communication occurs through-space rather than through-bond. In these very crowded complexes, the metal–metal interaction is essentially due to electrostatic effect which is expected to be dominant in determining the value of the related comproportionation constant K_c.

Stepwise oxidation of **83** with $AgSbF_6$ in dichloromethane showed the appearance of an absorption band around 5000 cm^{-1}, the intensity of which increased up to 2–3 equivalents of oxidant added, indicating the formation of **83**$^{2+}$ via **83**$^{+}$ and assigned to IVCT transitions. The electronic coupling H in **83**$^{+}$ and **83**$^{2+}$ (145 and 220 cm^{-1}, respectively) was estimated using the Hush relationship (eq. 6) with r = 6Å ($\tilde{\nu}_{max}$ = 4800, 4500 cm^{-1}, ε_{max} = 125, 280 M^{-1} cm^{-1} and $\Delta\tilde{\nu}_{1/2}$ = 3035, 3345), values typical of weakly coupled, class II, mixed valence cations.

A square of four electronically coupled sites containing two itinerant electrons is reasonably a useful building block for quantum cellular automata (QCA) devices.

The first example of an isolated four-metal, mixed-valence complex containing two mobile electrons in a square geometry, i.e. CpCo(Fc$_4$C$_4$)$^{2+}$ (**84**$^{2+}$), was fully characterized by Long and Fehlner,[81] a symmetrical square system containing two ferrocene and two ferrocenium moieties having properties suitable for use as a component for QCA circuits.

Though this system, based on the (η^4-cyclobutadiene)(η^5-cyclopentadieny1)Co platform (**84**) was early described by Raush[35] and promising data for the **84**$^{1+/2+/3+}$ relative to and IVCT bands in the visible and NIR region were reported, electrochemistry in dichloromethane/nBu$_4$NPF$_6$ was unsatisfactory and none of these ions were previously isolated.

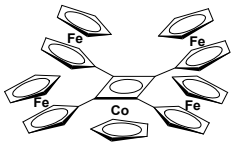

84

The cations **84**$^{+}$ and **84**$^{2+}$ were isolated and characterized. In particular, electrochemistry of **84** and NIR spectra of **84**$^{+}$ and **84**$^{2+}$ have been re-examined in a 1:1 mixture of CH_3CN. CV and SWV experiments in dichloromethane gave good resolution with evidence of three redox waves. In SWV, the unresolved wave at the most positive potential clearly evidenced the presence of a fourth peak ($E_{1/2}$ = –0.09, 0.08, 0.23, and 0.28 V vs Fc/Fc^{+}).

The bands observed for **84**$^{+}$ and **84**$^{2+}$ were assigned to IVCT transitions, that of **84**$^{2+}$ occurring at higher energy. The solvent dependence of $\tilde{\nu}_{max}$ and the Hush parameters calculated from the band energies, bandwidths, and intensities suggested electron localization, class II, behaviour in the Robin-Day classification.

In the solid state, two Fe^{II} and two Fe^{III} sites were observed in both the IR and Mössbauer spectra of **84**$^{+}$ and **84**$^{2+}$, indicating that these cations are valence trapped, class II, compounds on the 10^{-12} s IR time scale.

The valence trapping observed in the solid state suggests that **84**$^{2+}$ possesses properties that permit its use as a building block in molecular QCA cell.

A number *of meso* ferrocenyl porphyrins has been reported in literature.[82] The tetra(ferrocenyl) substituted porphyrin (**85**) has been prepared and investigated by Nemykin and Galloni, and is undoubtedly a potential candidate for application in QCA device,[40, 83] and a photoactive material for photoelectrochemical cells.[84]

The electrochemical properties of **85** were studied using CV, DPV and SWV methods in different combinations of solvent and supporting electrolyte. [83c.]

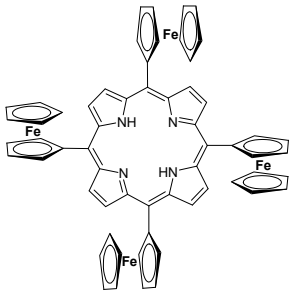

85

In particular, resolution of the redox events was obtained by using

the weakly coordinating nBu$_4$NB(C$_6$F$_5$)$_4$ as the supporting electrolyte in the low coordinating solvent dichloromethane. In this medium, the ferrocenyl-based oxidation resulted in four well separated one-electron oxidation processes at $E_{1/2}$ = –0.07, 0.15, 0.24 and 0.34 V vs Fc/Fc$^+$ in which the ΔE splitting between the first two waves displayed the largest value with respect those between the subsequent ones; similar results but with less pronounced ΔE splitting were observed in dichloromethane with the more coordinating nBu$_4$NPF$_6$ electrolyte ($E_{1/2}$ = –0.01, 0.08, 0.14 and 0.25 V vs Fc/Fc$^+$).

The increased wave separations, observed when the weakly coordinating anion B(C$_6$F$_5$)$_4^-$ was present in the supporting electrolyte, could be ascribed to the existence of significant electrostatic repulsion between the non-coordinated cationic centres, especially in the dication **85**$^{2+}$. On the other hand, the persistence of a ΔE splitting in traditional electrolyte containing the anions BF$_4^-$ or PF$_6^-$, which may react as nucleophiles with radical cations, corresponds approximately to the electronic communication in the absence of other significant factor.[29a]

Two processes are conceivable for the formation of **85**$^{2+}$, i.e. the oxidation of the second ferrocenyl group at an adjacent or opposite position relative to the first oxidized iron centre. Statistically, the oxidation of the adjacent substituent is more favoured. However, the electrostatic repulsion in the dication with the charges located at opposite positions should be reasonably less.

Spectroelectrochemical and chemical oxidation of **85** resulted in formation of the **85**$^+$, **85**$^{2+}$ and **85**$^{3+}$ mixed-valence species as well as of **85**$^{4+}$. The IVCT bands observed in the NIR region for **85**$^+$, **85**$^{2+}$ and **85**$^{3+}$ were analysed using the Hush model; the magnitudes of the electronic coupling H were in agreement with the class II character in the Robin-Day classification and indicative of trapped-valency. Valence localization of **85**$^+$ and **85**$^{2+}$ was also confirmed by MIR, Mössbauer and XPS data.

These remarkable properties prompted Galloni and Niemykin's groups to prepare and characterize novel tetra(ferrocenyl)porphyrin containing self-assembled monolayers (SAMs), and a preliminary investigation on their photocurrent generation efficiency.[84]

The electrochemical and optical properties of tetra(ferrocenyl) substituted thiophene, furan and pyrrole **86**–**89** were prepared and investigated by CV, SWV and in situ UV–vis/NIR spectroscopy by Lang.[42b–e]

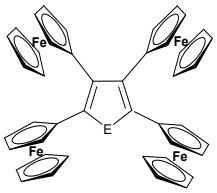

86, E = S
87, E = O
88, E= NMe
89, E= NPh

As the iron–iron distances in this series are almost equal, the electrostatic contribution to the ΔE separation were found comparable and, consequently, the trend of ΔE corresponded to the electronic communication.

The ΔE values between the first and the second redox waves followed the same trend observed in the bis(ferrocenyl) heterocycles **16**–**19**. However, as evidenced from solid state structure of **88**, the lack of coplanarity with the heterocyclic bridge due to the high steric hinderance of the adjacent ferrocenyl groups in **86**–**89** caused the decrease of ΔE values with respect to the bis(ferrocenyl) analogues. The separation of the successive redox events is mostly attributed to electrostatic effects.

The appearance of IVCT absorptions in the NIR region confirmed the existence of electronic coupling in the corresponding mono- and dicationic species and all mixed-valence compounds, except the class I thiophene-based **86**$^+$, were classified as class II systems according to Robin and Day.

The ΔE values between the first and the second redox waves correlated with the communication of the iron centres, namely the oscillator strength f of the IVCT transitions found in NIR region for **86**$^+$–**89**$^+$ (eq. 17 and 18) and allowed to estimate the electron transfer distance r, as for the series bis(ferrocenyl) heterocycles **16**$^+$–**24**$^+$. The electronic coupling in tetraferrocenyl heterocycles **86**$^+$–**88**$^+$ was found much lower than that observed in the bis(ferrocenyl) derivatives **16**$^+$–**18**$^+$. This could be attributed to the decreased coplanarity of the ferrocenyl group with the central heterocycles due to the higher steric demand in the more crowded **86**$^+$–**88**$^+$ series.

Electrochemical and optical investigations on linear tetra(ferrocenyl) systems were reported by Meyer[67] (**56**), Nishihara[68] (**59**) and Geiger[70] (**64**) (see the discussion in the previous Section). The position of the subsequent positive charges and the electrochemical characteristics in the mono and polycationic species depended of the interplay of the electrostatic and energetic factors along the chain of these multi(ferrocenyl) oligomers. In all the cases for which an absorption band was observed in NIR region, the typical characteristics of Class II mixed-valence complexes were observed.

Penta(ferrocenyl) complexes

Penta(ferrocenyl) complexes are quite rare due to synthetic difficulties.

Linear penta(ferrocenyl) complexes **60** and **65** displayed electrochemical and optical behaviour quite similar to that found along the corresponding series of compounds with increasing number of concatenated ferrocenyl groups (see the discussion in the previous Section).

Vollhardt synthesized and characterized the first "star-shaped" oligocyclopentadienyl metal complexes, among these the penta(ferrocenyl) derivatives **90**–**92**.[85]

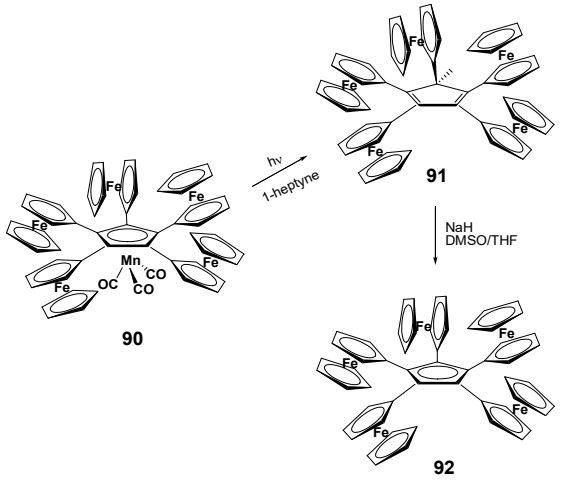

90 **91** **92**

The lack of coplanarity of the central cyclopentadienyl, evidenced by X-ray structure, attenuates but does not remove intermetallic interaction in **90**, as indicated by CV data in CH_2Cl_2 / nBu$_4$NPF$_6$, which displayed three oxidation waves at $E_{1/2}$ = 0.05, 0.17 and 0.28 V vs Fc/Fc$^+$ in a 2e/1e/1e sequence.

Compared to **90**, the molecule of **91** is much released of strain. Nevertheless, the ferrocenyl bonded to the sp^3-carbon is oriented out of the mean plane of the cyclopentadiene. Comparison of the CV data ($E_{1/2}$ = –0.11, 0.17 and 0.33 V) with that of **90**, revealed clearly the effect of isolating electronically the sp^3-bonded ferrocenyl from the rest of the molecule.

The anion **92** showed three oxidation steps at $E_{1/2}$ =–1.25, 0.20, and 1.20 V, reflecting the transitions from anion → radical → cation (possibly ferrocenyl centred) → dication.

Similarly to what observed in the very crowded EFc$_4$ complexes, we believe that the metal–metal interaction is essentially due to electrostatic effect. Unfortunately, neither the effect of the weakly coordinating nBu$_4$NB(C$_6$F$_5$)$_4$ on the wave multiplicity and separation, or the presence of mixed-valence cations were verified.

The advances in manipulation of single molecules[86] have stimulated much interest in the synthesis of molecular machines,[87] as nanowheels,[88] nanocars,[89] and nanogears.[90]

Recently, Rapenne and Launay reported the synthesis of ruthenium(II) 1,2,3,4,5-penta(*p*-ferrocenylphenyl)-cyclopentadienyl-hydrotris(indazolyl) borate (**93**), a piano stool complex described as the active part of a potential organometallic molecular machine, i.e. a rotor composed by five terminal ferrocenyl groups connected to a tripodal ligand (stator) by means of a ruthenium(II) centre. This system may be considered as the heart of a future molecular motor.[91]

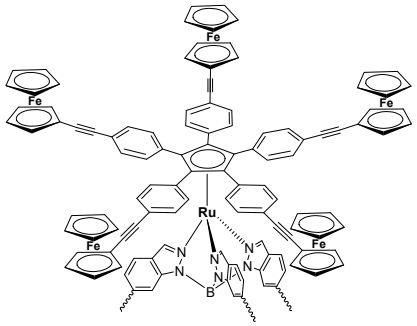

93

In **93**, there is essentially one degree of freedom: the rotation of the upper part with respect to the lower one. All the requirements for such a molecule to operate as a molecular motor were verified: (i) within CV experiments in CH_2Cl_2 containing nBu$_4$NPF$_6$, the reversible oxidation potential of ferrocenyl groups occurred at the same potential (0.52 V vs SCE), lower than that of the ruthenium centre (0.82 V vs SCE) which consequently remains inert towards the redox cycles of the terminal ferrocenyl groups; (ii) no IVCT band was observed by spectroelectrochemistry in the vis-NIR region, showing that the electrostatic interaction and electronic coupling between two adjacent metal centres are absent or very weak. Electronic coupling is here an undesirable phenomenon since it would allow intramolecular charge transfer between neighbouring ferrocene centres, without actual turning of the rotor; (iii) the rotation barrier of the rotor was very low, as shown by NMR and DFT calculations.

The possibility to observe and exploit a controlled rotation on a surface was also verified.[92]

Hexa(ferrocenyl) complexes

Electrochemical and optical investigations on linear hexa(ferrocenyl) systems were reported by Nishihara[68] (**59**) and Geiger[70] (**66**) and discussed in the previous Sections.

As far as "star-shaped" hexaferrocenyl complexes are concerned, Vollhardt was able to synthesize the elusive for decades hexaferrocenylbenzene (**94**).[93]

The six bulky ferrocenyl groups give the molecule an extremely crowded structure, as evidenced by X-ray analysis. The C$_5$H$_4$ substituents deviate considerably from coplanarity with the benzene ring, with dihedral angles falling into two alternating groups averaging of 30.8 and –81.9°. In addition, the benzene ring adopts a chair conformation caused by the perferrocenylation.

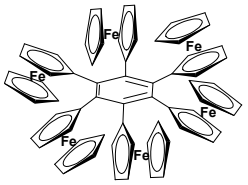

94

The CV in CH_2Cl_2 / nBu$_4$NPF$_6$ exhibited well separated redox waves at $E_{1/2}$ = –0.16, –0.03 and 0.22 V vs Fc/Fc$^+$ in a 1e/2e/3e sequence. Taking into account the lack of planarity and the close proximity of the ferrocenyl groups, we believe that the separation of these redox events is mostly owed to electrostatic effects. Regrettably, the effect of the weakly coordinating nBu$_4$NB(C$_6$F$_5$)$_4$ and the existence of mixed-valence states were not examined.

A family of rigid "star-shaped" ferrocenyl-terminated complexes has been synthesized by Astruc, including hexa(ferrocenylethynyl)benzene complexes (**95**), also containing permethylated (**96**) and monomethylated (**97**) cyclopentadienyl ligands.[29]

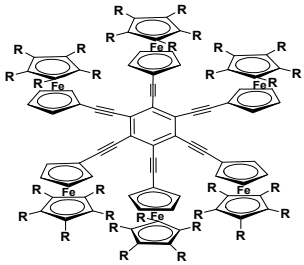

95, R = H
96. R =CH$_3$

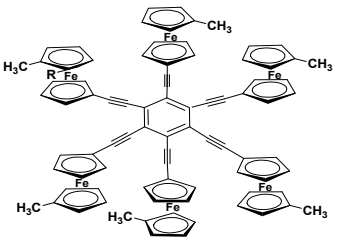

97

The CVs of **95**–**97** in CH_2Cl_2 showed a single wave when nBu$_4$NPF$_6$ was used as the supporting electrolyte, as well the CVs of the structurally related bis(ferrocenyl) **6p** and tris(ferrocenyl) **47** complexes.

The lack of wave splitting ΔE was attributed to the absence of significant intramolecular communication between the irons. The CVs were also recorded with nBu$_4$NB(C$_6$F$_5$)$_4$ as supporting electrolyte, whose advantages were discussed above. While the CV of the binuclear **6p** still showed a single wave, those of the trinuclear **47** and hexanuclear **95** split into three well-separated one-electron and two-electron waves, respectively, meaning that the splitting, might not result from electronic communication among the redox centres, but from electrostatic effects due to the scarce ion pairing capability of B(C$_6$F$_5$)$_4^-$ towards the oxidized compound with respect to traditional anions.

The electrostatic effect suggested the distinction among the three two-electron oxidation steps of **95** on the basis of the large differences of the electrostatic interaction in the *ortho*, *meta*, and *para* positions (Figure 9).

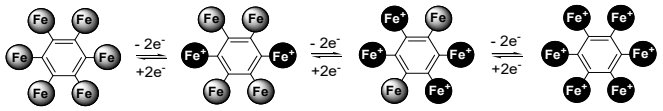

Fig. 9 Oxidation mechanism of **95** in the presence of nBu$_4$NB(C$_6$F$_5$)$_4$ in CH_2Cl_2.

The CV of **96** with nBu$_4$NB(C$_6$F$_5$)$_4$ resulted in a broad overlap of not resolved waves. Interestingly, the CV of the monomethylated **97** was more clearly resolved and six single-electron oxidation waves could be distinguished. This result was attributed to the perturbation of the ion-pairing strength by the presence of a single methyl group on each ferrocenyl redox centre.

The lack of spectroscopic studies on the mixed-valent behaviour of the cationic derivatives prevents any ultimate conclusion on the nature, electrostatic and/or electronic, of the metal–metal interaction.

The hexa(*p*-ferrocenylphenyl)benzene (**98**) was prepared by Chebny[94] The CV of **98** in CH_2Cl_2 and nBu$_4$NPF$_6$ as the supporting electrolyte showed only a single reversible wave. Redox titration confirmed that it ejects six electrons at the same potential. The incremental addition of the naphthalene cation radical as a robust one-electron oxidant afforded the bright green hexacation **98**$^{6+}$ which showed a band in the NIR region ($\tilde{\nu}_{max}$ = 9050 cm^{-1}, ε_{max} = 1400 M^{-1} cm^{-1}) in dichloromethane, typical of a ligand-to-metal charge transfer (LMCT) transition.

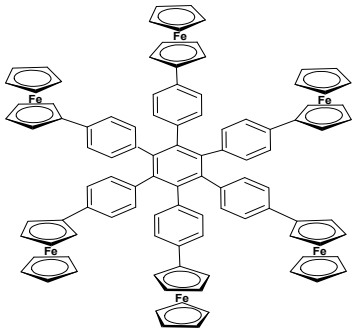

98

The authors suggested that the ferrocenyl groups are not electronically coupled. However, the use of the weakly coordinating nBu$_4$NB(C$_6$F$_5$)$_4$, which may be able to separate the single oxidation steps allowing to the existence of mixed- valency and IVCT bands, was not considered.

The last proposed molecules of this tracking shot on the multi(ferrocenyl) family are the 3,3′,4,4′,5,5′-hexaferrocenyl-2,2′-bithiophene (**99**) and the related 3,4,5-tris(ferrocenyl)thiophene (**100**), recently prepared by Lang.[42a,95]

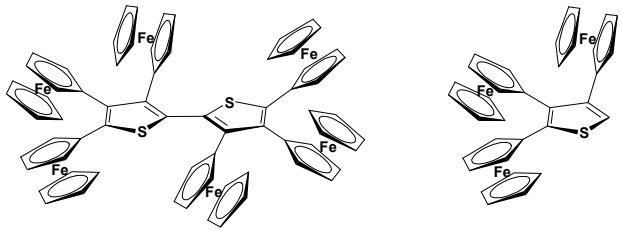

99 **100**

Their electrochemical and electronic properties were defined by CV and SWV measurements and in situ UV−vis/NIR spectroelectrochemistry. Three successive one-electron oxidation at $E_{1/2}$ = −0.12, 0.15 and 0.43 V vs Fc/Fc$^+$ were observed for the trinuclear **100** in dichloromethane solutions using nBu$_4$NB(C$_6$F$_5$)$_4$ as supporting electrolyte. The hexanuclear **99** dispalyed five redox processes at $E_{1/2}$ = − 0.165, 0.26, 0.49, 0.65 and 0.80 V vs Fc/Fc$^+$ in anisole/nBu$_4$NB(C$_6$F$_5$)$_4$, the first one corresponded to two one-electron events close together, followed by four separated one-electron waves. Stepwise oxidation of the ferrocenyl groups was obtained by spectroelectrochemistry. Surprisingly, while mono-oxidated **100**$^+$ and **100**$^{2+}$ lead to the appearance of an IVCT absorption band at 6628 cm^{-1} and 7520 cm^{-1}, respectively, with characteristics typical of a mixed-valent Class II system, the absence of low-energy bands in the NIR region for **99**$^{n+}$ (n = 1–5) indicated that the ferrocenium units essentially communicate electrostatically with each other, and the positive charges are mainly localized on the ferrocenium moieties, similarly to what found for the supercrowded tetraferrocenyl thiophene cation **86**$^+$.

Conclusions

The aim of this review is that to provide a perspective on the family of multi(ferrocenyl) complexes with a number of ferrocenes from two to six. In particular, for molecules with more than two metal groups, three molecular shapes were considered, namely star, linear and cyclic systems.

Specifically, we have focused our attention on those key complexes which were employed as precursors of mixed-valence cations displaying mainly electrostatic and electronic interactions that in some cases cooperate in determining the overall metal–metal communication. We have tried to identify the experimental approaches principally employed to highlight the contribution of these two effects, and here summarized with some warnings and “precautions for use”:

- the thermodynamic stability of the mixed-valence state can be easily calculated from electrochemical data; larger and resolvable ΔE between successive redox events are indicative of increased K_c values;
- the ΔE splitting between two CV waves of two equivalent redox centres, observed using traditional supporting electrolyte containing BF_4^- and PF_6^- which may react as nucleophiles with radical cations, could correspond approximately to the electronic

communication in the absence of other significant factors, but undetectable or small ΔEs are not diagnostic of a negligible communication;
- if ΔE splitting or increased wave separation are observed with supporting electrolytes containing weakly coordinating anions such as $B(C_6F_5)_4^-$, these effects may be attributed to significant electrostatic repulsion between the positive charges in the dication;
- warning is needed in the interpretation of electrochemical data due to the dependence of ΔE splitting on the nature of the solvent and supporting electrolyte; more diagnostic are optical investigations in the NIR region where mixed-valence species typically absorb.

Many fascinating examples of multi(ferrocenyl) complexes are reported in literature, a few of which are promising candidate for application as molecular devices such as quantum cellular automata or sensors. In this perspective, the experimental validations summarized above and described by several studies here reviewed represent the minimal requisites for the best comprehension of the nature of the metal–metal interaction.

Acknowledgements

Financial support by Italian MIUR (ex-60% grants) is gratefully acknowledged.

Notes and references

1 (a) J. Weiss, *Coord. Chem. Rev*. 2010, **254**, 2247; (b) Nano and Molecular Electronics Handbook and S. E. Lyshevski, Ed. CRC Press: New York, 2007; (c) H. Bayley, *Nature* 2010, **467**, 164; (d) F. Giacalone and N. Martin, *Adv. Mater.*, 2010, **22**, 4220; (e) M. Jurow, A. E. Schuckman, J. D. Batteas and C. M. Drain, *Coord. Chem. Rev.* 2010, **254**, 2297; (h) A. Chung, J. Deen, J.-S. Lee and M. Meyyappan, *Nanotechnology* 2010, **21**, 412001; (f) V. Balzani, V. Credi and M. Venturi, *Nanotoday*, 2007, **2**, 18.

2 (a) T. Fukino, N. Fujita and T. Aida, *Org. Lett.* 2010, **12**, 3074; (c) I. Manners, *Science* 2001, **294**, 1664; (d) L. De Cola and P. Belser, In *Electron Transfer in Chemistry*, Ed. V. Balzani, Wiley-VCH: Weinheim, 2001, Vol 5, p 97; (e) M. N. Paddow-Row, In *Electron Transfer in Chemistry*, Ed. V. Balzani, Wiley-VCH: Weinheim, 2001, Vol 2, p 179; (f) C. Joachim, J. K. Gimzewski and A. Aviram, *Nature*, 2000, **408**, 541.

3 (a) Fabre, *Acc. Chem. Res.* 2010, **43**, 1509; (b) W. Kaim and G. K. Lahiri, *Angew. Chem., Int. Ed.* 2007, **46**, 1778; (c) W. Kaim and B. Sarkar, *Coord. Chem. Rev.* 2007, **251**, 584; (d) M. H. Chisholm and N. J. Patmore, *Acc. Chem. Res.* 2007, **40**, 19.

4 (a) D. Astruc, C. Ornelas and J. Ruiz Aranzaes, *J. Inorg. Organomet. Polym. Mater.* 2008, *18*, 4; (b) D. O. Cowan and C. LeVanda, J. Park and F. Kaufman, *Acc. Chem. Res.* 1973, **6**, 1; (c) M. Wagner, *Angew. Chem., Int. Ed.* 2006, **45**, 5916; (d) J. S. Miller and A. J. Epstein, *Angew. Chem., Int. Ed. Engl.*, 1994, **33**, 385; (e) S. Barlow, *Inorg. Chem.* 2001, **40**, 7047; (f) G. Giuffrida and S. Campagna, *Coord. Chem. Rev.* 1994, **135-136**, 517; (g) A. Donoli, A. Bisello, R. Cardena, A. Ceccon, M. Bassetti, A. D'Annibale, C. Pasquini, A. Raneri and S. Santi, *Inorg. Chim. Acta* 2011, **374**, 442; (h) S. Steffens, M. H. Prosenc, J. Heck, I. Asselberghs and K. Clays, *Eur.*, *J. Inorg. Chem.*, 2008, 1999.

5 (a) P. Stepnicka, *Ferrocenes: Ligands, Materials and Biomolecules*, Ed. Wiley-VCH: Chichester, England, 2008; (b) K. Kowalski, M. Linseis, R. F. Winter, M. Zabel, S. Zalis, H. Kelm, H.-J. Kruger, B. Sarkar and W. Kaim, *Organometallics*, 2009, **28**, 4196; (c) T. Nakaya, K. Namiki, M. Murata, K. Kanaizuka, M. Kurashina, T. Fujita and H. Nishihara, *J. Inorg. Organomet. Polym. Mater.*, 2008, **18**, 124; (d) R. Zhang, Z. Wang, Y. Wu, H. Fu and J. Yao, *Org. Lett.*, 2008, **10**, 3065; (e) P. Debroy and S. Roy, *Coord. Chem. Rev.*, 2007, **251**, 203; (f) A. Caballero, A. Tàrraga, M. D. Velasco, A. Espinosa and P. Molina *Org. Lett.*, 2005, **7**, 3171.

6 A. Heckmann and C. Lambert, *Angew. Chem., Int. Ed.* 2012, **51**, 326.

7 (a) C. Creutz and H. Taube, *J. Am. Chem. Soc.,* 1969, **91**, 3988; (b) C. Creutz and H. Taube, *J. Am. Chem. Soc.*, 1973, **95**, 1086.

8 (a) B. Sarkar, R. H. Laye, B. Mondal, S. Chakraborty, R. L. Paul, J. C. Jeffery, V. G. Puranik, M. D. Ward and G. K. Lahiri, *J. Chem. Soc. Dalton Trans.*, 2002, **9**, 2097; (b) C. B. Evans, M. L. Nacklicki, A. R. Rezvani, C. A. White, V. V. Kondratiev and R. J. Crutchley, *J. Am. Chem. Soc.* 1998, **120**, 13096.

9 (a) D. O. Cowan and F. Kaufman, *J. Am. Chem. Soc.*, 1970, **92**, 219; (b) C. LeVanda, K. Bechgaard and D. O. Cowan, , *J. Org. Chem.*, 1976, **41**, 2700; (c) C. LeVanda, K. Bechgaard, D. O. Cowan, U. T. Mueller-Westerhoff, P. Eilbracht, G. A. Candela and R. L. Collins, *J. Am. Chem. Soc.* 1976, **98**, 3181.

10 (a) M. D. Ward, *Chem, Soc. Rev.*, 2005, 121; (b) S. Barlow and D. O'Hare, *Chem. Rev.*, 1997, **97**, 637; (c) Launay, J.-P. *Chem. Soc. Rev.*, 2001, **30**, 386; (c) H. Nishihara, *Bull. Chem. Soc. Jpn.*, 2001, **74**, 19; (d) P. L. Low, R. L. Roberts, R. L. Cordiner and F. Hartl, *J. Solid State Electrochem.*, 2005, **9**, 717; (e) D. M. D'Alessandro and F. R. Keene, *Chem. Rev.*, 2006, **106**, 2270; (f) P. J. Low, *Coord. Chem. Rev.*, 2013, **257**, 1507.

11 M. B. Robin and P. Day, *Adv. Inorg. Chem. Radiochem.* 1967, **10**, 247.

12 (a) N. S. Hush, *Prog. Inorg. Chem.*, 1967, **8**, 391; (b) N. S. Hush, *Electrochim. Acta* 1968, **13**, 1005; (c) G. C. Allen and N. S. Hush, *Prog. Inorg. Chem.*, 1967, **8**, 357; (d) N. S. Hush, *Trans. Faraday Soc.*, 1961, **57**, 557; (e) P. Day and N. S. Hush, R. J. H. Clark, *Philos. Trans. R. Soc. A*, 2008, **366**, 5; (f) R. A. Marcus, *J.*

Chem. Phys., 1956, **24**, 966; (g) R. A. Marcus, *Disc. Faraday Soc.*, 1960, **29**, 21; (h) R. A. Marcus, *J. Chem. Phys*. 1965, **43**, 679; (i) R. A. Marcus, *J. Electroanal. Chem.*, 1997, **438**, 251.
13 M. Al-Noaimi, G. P. A. Yap and R. J. Crutchley, *Inorg. Chem.*, 2004, **43**, 1770.
14 (a) N. S. Hush, *Coord. Chem. Rev.*, 1985, **64**, 135; (b) B. S. Brunschwig, C. Creutz and N. Sutin, *Chem. Soc. Rev.*, 2002, **31**, 168.
15 C. Creutz, Prog. *Inorg. Chem.*, 1983, **30**, 1.
16 R. J. Crutchley, *Adv. Inorg. Chem.*, 1994, ***41***, 273.
17 (a) C. Creutz, M. D. Newton and N. Sutin, *J. Photochem. Photobiol. A*, 1994, **82**, 47; (b) R. J. Cave and M. D. Newton, *Chem. Phys. Lett.*, 1996, **249**, 15.
18 D. E. Richardson and H. Taube, *Coord. Chem. Rev.* 1984, **60**, 107.
19 (a) P. Chen and T. J. Meyer, *Chem. Rev.* 1998, **98**, 1439; (b) K. D. Demadis, C. M. Hartshom and T. J. Meyer, *Chem. Rev.*, 2001, **101**, 2655.
20 J. E. Sutton, P. M. Sutton and H. Taube, *Inorg. Chem.* 1979, **18**, 1017.
21 (a) F. Ammar and J.-M. Savéant, *J. Electroanal. Chem.* 1973, **43**, 115; (b) D. E. Richardson and H. Taube*, Inorg. Chem.* 1981, **20**, 1287.
22 (a) W. E. Geiger and F. Barriére*, Acc. Chem. Res.*, 2010, **43**, 1030; (b) F. Barriére and W. E. Geiger, *J. Am. Chem. Soc.*, 2006, **128**, 3980; (c) F. Barriére, N. Camire, W. E. Geiger, U. T. Mueller-Westerhoff and R. Sanders, *J. Am. Chem. Soc.*, 2002, **124**, 7262; (d) D. M. D'Alessandro and F. R. Keene, *Dalton Trans.*, 2004, 3950; (e) S. Santi, L. Orian, C. Durante, A. Bisello, F. Benetollo, L. Crociani, P. Ganis and A. Ceccon, *Chem. Eur. J.* 2007, **13**, 1955; (f) S. Santi, L. Orian, C. Durante, E. Z. Bencze, A. Bisello, A. Donoli, F. Benetollo, L. Crociani and A. Ceccon, *Chem. Eur. J.* 2007, **13**, 7933; (g) D. M. D'Alessandro and F. R. Keene, *Dalton Trans.*, 2004, 3950.
23 (a) P. Hapiot, L. D. Kispert, V. V. V. Konovalov and J.-M. Savéant, *J. Am. Chem. Soc.*, 2001, **123**, 6669; (b) S. I. Ghazala, F. Paul, L. Toupet, T. Roisnel, P. Hapiot and C. Lapinte, *J. Am. Chem. Soc.*, 2006, **128**, 2463; (c) D. P. Arnold, R. D. Hartnell, G. A. Heath, L. Newby and R. D. Webster, *Chem. Commun.*, 2002, **754**; (d) A.-C. Ribou, J.-P. Launay, K. Takahashi, T. Nihara, S. Tarutani and C.W. Spangler, *Inorg. Chem.*, 1994, **33**, 1325.
24 J. R. Reimers and N. Hush, *Inorg. Chem.* 1990, **29**, 3686.
25 B. S. Brunschwig and N. Sutin, *Coord. Chem. Rev.*, 1999, **187**, 233.
26 A.-C. Ribou, J.-P. Launay, M. L. Sachtleben, H. Li and C.W. Spangler, *Inorg. Chem.*, 1996, **35**, 3735.
27 H. M. McConnell, *J. Chem. Phys.*, 1961, **35**, 508.
28 C. Patoux, C. Coudret, J.-P. Launay, C. Joachim and A. Gourdon, *Inorg. Chem.*, 1997, **36***,* 5037.
29 (a) A. K. Diallo, C. Absalon, J. Ruiz and D. Astruc *J. Am. Chem. Soc.*, 2011, **133**, 629; (b) A. K. Diallo, J.-C. Daron, F. Varret, C. J. Ruiz, D. Astruc, *Angew. Chem. Int. Ed.*, 2009, **48**, 3145.
30 H. Fink, N. L. Long, A. J. Martin, G. Opromolla, A. J. P. White, D. J. Williams and P. Zanello, *Organometallics*, 1997, **16**, 2646.
31 (a) M. Iyoda, T. Kondo, T. Okabe, H. Matsuyama, S.Sasaki and Y. Kuwatani, *Chem. Lett.*, 1997, 35. (b) S. Fiorentini, B. Floris, S. Fiorentini, B. Floris, P. Galloni, F. Grepioni, M. Polito and P. Tagliatesta, *Eur. J. Org. Chem.*, 2006, 1726.
32 C. Lapinte, *J. Organomet. Chem.*, 2008, **693**, 793, and references therein.
33 A. Donoli, A. Bisello, R. Cardena, F. Benetollo, A. Ceccon and S. Santi, *Organometallics*, 2011, **30**, 1116.
34 V. Gonzalo, C. Coudret, C. Patoux and J.-P. Launay, *C. R. Chim.*, 1999, **2**, 321.
35 M. D. Rausch, F. A. Higbie, G. F. Westover, A. Clearfield, R. Gopal, J. M. Troup and I. Bernal, *J. Organomet. Chem*, **1978**, **149**, 245. J. Kotz, G. Neyhart, W. J. Vining and M. D. Rausch, *Organometallics*, 1983, **2**, 79.
36 P. D. W. Boyd, A. K. Burrell, W. M. Campbell, P. A. Cocks, K. C. Gordon, G. B. Jameson, D. L. Officer and Z. Zhao, *Chem. Commun.*, 1999, 637.
37 S.W. Rhee, Y.H. Na, Y. Do and J. Kim, , *Inorg. Chim. Acta*, 2000, **309**, 49.
38 N. L. Loim, N. V. Abromova and V. I. Sokolov, *Mendeleev Commun.*, 1996, 46.
39 A. Auger and J. C. Swarts, *Organometallics*, 2007, **26**, 102.
40 V. N. Nemykin, G. T. Rohde, C. D. Barrett, R. G. Hadt, J. R. Sabin, G. Reina, P. Galloni and B. Floris, *Inorg. Chem*., 2010, **49**, 7497.
41 C. H. Devillers, A. Milet, J.-C. Moutet, J. Pécaut, G. Royal, E. Saint-Aman and C. Bucher, *Dalton Trans.*, 2013, **42**, 1196.
42 (a) J. M. Speck, R. Claus, A. Hildebrandt, T. Rüffer, E. Erasmus, L. van As, J. C. Swarts and H. Lang, *Organometallics*, 2012, **31**, 6373; (b) A. Hildebrandt, T. Rüffer, E. Erasmus, J. C. Swarts and H. Lang, *Organometallics*, 2010, **29**, 4900; (c) A. Hildebrandt, D. Schaarschmidt, R. Claus and H. Lang, *Inorg. Chem.* 2011, **50**, 10623; (d) A. Hildebrandt, D. Schaarschmidt, H. Lang, *Organometallics*, 2011, **30**, 556; (e) A. Hildebrandt and H. Lang, *Dalton Trans.* 2011, **40**, 11831.
43 A. Hildebrandt and H. Lang, *Organometallics*, 2013, **32**, 5640.
44 (a) B. Jin, F. Tao and P. Liu, *J. Electroanal. Chem.*, 2008, **624**, 179. (b) Y.-Q. Hu, L.-M. Han, H.-L. Hong and R.-J. Xie, *J. Coord. Chem.*, 2013, **66**, 3481.
45 D. Miesel, A. Hildebrandt, M. Korb, P. J. Low and H. Lang, *Organometallics*, 2013, ***32***, 2993.
46 S. C. Jones, S. Barlow and D. Hare, *Chem. Eur. J.* 2005, **11**, 4473.
47 (a) V. V. Dement'ev, F. Cervantes-Lee, L. Parkanyi, H. Sharma, K. H. Pannell, M. T. Nguyen and A. F. Diaz, *Organometallics*, 1993, **12**, 1983; (b) D. A. Foucher, C. H. Honeyman, J. M.

Nelson, B. Z. Tang and I. Manners, *Angew. Chem. Int. Ed. Engl.* 1993, **32**, 1709.
48 H. A. Fogarty, D. L. Casher, R. Imhof, T. Schepers, D. W. Rooklin and J. Michl, *Pure Appl. Chem*., 2003, **75**, 999; (b) D. A. Foucher, B. Z. Tang and I. Manners, *J. Am. Chem. Soc*., 1992, **114**, 6246.
49 A. Donoli, V. Marcuzzo, A. Moretto, M. Crisma, C. Toniolo, R. Cardena, A. Bisello and S. Santi, *Biopolymers*, 2013, **100**, 14.
50 A. Donoli, V. Marcuzzo, A. Moretto, M. Crisma, C. Toniolo, R. Cardena, A. Bisello and S. Santi, *Org. Lett.*, 2011, **13**, 1282.
51 S. Antonello, F. Formaggio, A. Moretto, C. Toniolo and F. Maran, *J. Am. Chem. Soc.*, 2003, **125**, 2874.
52 H. Sun, J. Steeb and A. E. Kaifer, *J. Am. Chem. Soc.*, 2006, **128**, 2820.
53 (a) C. S. Lent, P. D. Tougaw, W. Porod and G. H. Bernstein, *Nanotechology,* 1993, **4**, 49. (b) A. O. Orlov, I. Amlani, G. H. Berstein, C. S. Lent and G. L. Snider, *Science*, 1997, **277**, 928. (c) C. S. Lent, *Science* 2000, **288**, 1597.
54 (a) A. Aviram, M. A. Ratner, *Chem. Phys. Lett.* 1974, **29**, 277; (b) J. Jortner and M. A. Ratner, *Molecular Electronics*; Blackwell Science: Oxford, 1997.
55 V. Arima, M. Iurlo, L. Zoli, S. Kumar, M. Piacenza, F. Della Sala, F. Matino, G. Maruccio, R. Rinaldi, F. Paolucci, M. Marcaccio, P. G. Cozzi and A. P. Bramanti, *Nanoscale*, 2012, **4**, 813.
56 L. Bonci, M. Gattobigio, G. Iannaccone and M. Macucci, *J. Appl. Phys.*, 2002, **92**, 3169.
57 (a) Y.-K. Lim, L. Wallace, J. C. Bollinger, X. Chen and D. Lee, *Inorg. Chem.* 2007, **46**, 1694; (b) S. Fiorentini, B. Floris, P. Galloni, F. Grepioni, M. Polito and P. Tagliatesta, *Eur. J. Org. Chem.* 2006, 1726 (d) S. Barlow, V. J. Murphy, J. S. O. Evans and D. O'Hare, *Organometallics* 1995, **14**, 3461; (e) G. M. Brown, T. H. Meyer, D. O. Cowan, C. Le Vanda, F. Kaufman, P.V. Roling and M. D. Raush, *Inorg. Chem.* 1974, **14**, 506.
58 M. Herberhold. In *Ferrocenes* (Eds.: A. Togni, T. Hayashi) Wiley-VCH: Weinheim, 1995, p. 236.
59 F. Delgado-Pena, D. R. Talham and D. O. Cowan, *J. Organomet. Chem*., 1983, **253**, C43.
60 M. Herrero, R. Sevilla, C. M. Casado, J. Losada, P. García-Armada, A. Rodríguez-Diéguez, D. Briones and B. Alonso, *Organometallics*, 2013, **32**, 5826.
61 W. E. Britton, R. Kashyap, M. El-Hashash and M. El-Kady, *Organometallics* 1986**, 5**, 1029.
62 M. Herberhold, M. Ellinger, U. Thewalt and F. Stollmaier, *Angew. Chem., Int. Ed. Engl.,* 1982*,* **21**, 74.
63 U. Pfaff, A. Hildebrandt, D. Schaarschmidt, T. Hahn, S. Siebing, J. Kortus and H. Lang, *Organometallics*, 2012, **31**, 6761.
64 O. Kahn, *MolecularMagnetism*, VCH: New York, 1994, p. 241.
65 A. Donoli, A. Bisello, R. Cardena, C. Prinzivalli and S. Santi, *Organometallics*, 2013, **32**, 1029.
66 T. J. Katz and W. Ślusarek*, J. Am. Chem. Soc.*, 1980, **102**, 1058.
67 G. M. Brown and T. J. Meyer, D. O. Cowan, C. LeVanda, F. Kaufman, B. P. V. Roling, M. D. Rausch, *Inorg. Chem.,* 1975, **14***,* 506*.*
68 (a) K. Aoki, J. Chen, H. Nishihara and T. Hirao, *J. Electroanal. Chem.*, 1996, **416**, 151; (b) T. Horikoshi, K. Kubo and H. Nishihara, *J. Chem. Soc., Dalton Trans.*, 1999, 3355; (c) H. Nishihara and T. Horikoshi, *Synth. Met.*, 1999, **102**, 1523.
69 (a) K. Aoki and J. Chen, *J. Electroanal. Chem. Interfacial Electrochem.*, 1995, **380**, 35; (b) K. Aoki, J. Chen, H. Nishihara and T. Hirao, *J. Electroanal. Chem. Interfacial Electrochem*., 1996, **416**, 151.
70 R. Rulkens, A. J. Lough, I. Manners, S. R. Lovelace, C. Grant and W. E. Geiger, *J. Am. Chem. Soc.*, 1996, **118**, 12683.
71 M. J. Powers and T. J. Meyer, *J. Am. Chem. Soc.*, 1978, **100**, 4393.
72 U. H. F. Bunz, G. Roidl, M. Altmann, V. Henkelmann and K. D. Shimizu, *J. Am. Chem. Soc.*, 1999, **121**, 10719.
73 S. Santi, L. Orian, A. Donoli, A. Bisello, M. Scapinello, F. Benetollo, P. Ganis and A. Ceccon, *Angew. Chem., Int. Ed.*, 2008, **47**, 5331.
74 F. Scandola, R. Argazzi, C. A. Bignozzi, C. Chiorboli, M. T. Indelli and M. A. Rampi, *Coord. Chem. Rev.*, 1993, **125**, 283.
75 S. Santi, L. Orian, C. Durante, E. Z. Bencze, A. Bisello, A. Donoli, A. Ceccon, F. Benetollo and L. Crociani, *Chem. Eur. J.*, 2007, **13**, 7933.
76 M. J. MacLachlan, A. J. Lough, W. E. Geiger and I. Manners, *Organometallics*, 1998, **17**, 1873.
77 K. Jacob, N. Seidel, F. Voigt, A. Fischer, C. Pietzsch, J. Holecek, A. Lycka, M. Fontani, E. Grigiotti and P. Zanello, *J. Prakt. Chem.*, 2000, **342**, 574.
78 D. O. Cowan, P. Shu, F. L. Hedberg, M. Rossi and T. J. Kistenmacher, *J. Am.Chem. Soc.*, 1979, **101**, 1304.
79 M. J. Cohn, M. D. Timken and D. N. Hendrickson, *J. Am. Chem. Soc*., 1984, **106**, 6683.
80 D. Siebler, C. Förster, T. Gasi and K. Heinze, *Chem. Commun.*, 2010, **46**, 4490.
81 (a) J. Y. Jiao, G. J. Long, L. Rebbouh, F. Grandjean, A. M. Beatty and T. P. Fehlner, *J. Am. Chem. Soc.*, 2003, **125**, 7522; (b) J. Y. Jiao, G. J. Long, F. Grandjean, A. M. Beatty and T. P. Fehlner, *J. Am. Chem. Soc.*, 2005, **127**, 17819.
82 For a comprehensive literature, see 41 and reference therein.
83 (a) V. N. Nemykin, C. D. Barrett, R. G. Hadt, R. I. Subbotin, A. Y. Maximov, E. V. Polshin and A. Y. Koposov, *Dalton Trans.*, 2007, 3378; (b) V. N. Nemykin, P. Galloni, B. Floris, C. D. Barrett, R. G. Hadt, R. I. Subbotin, A. G. Marrani, R. Zanonic and N. M. Loim, *Dalton Trans.*, 2008, 4233; (c) V. N. Nemykin, G. T. Rohde, C. D. Barrett, R. G. Hadt, C. Bizzarri, P. Galloni, B. Floris, I. Nowik, R. H. Herber, A. G. Marrani, R. Zanoni and N. M. Loim, *J. Am. Chem. Soc.*, 2009, **131**, 14969.
84 A. Vecchi, E. Gatto, B. Floris, V. Conte, M. Venanzi, V. N. Nemykin and P. Galloni, *Chem. Commun.*, 2012, **48**, 5145.

85 Y. Yu, A. D. Bond, P. W. Leonard, K. P. C. Vollhardt and G. D. Whitener, *Angew. Chem. Int. Ed.*, 2006, **45**, 1794
86 F. Moresco, *Phys. Rep.*, 2004, **399**, 175, and references therein.
87 (a) V. Balzani, A. Credi and M. Venturi, *Molecular Devices and Machines–A Journey into the Nano World*, Wiley–VCH, Weinheim, 2003; (b) G. Rapenne, *Org. Biomol. Chem.*, 2005, ***3***, 1165.
88 L. Grill, K. H. Rieder, F. Moresco, G. Rapenne, S. Stojkovic, X. Bouju and C. Joachim, *Nat. Nanotechnol.*, 2007, **2**, 95.
89 (a) Y. Shirai, Y. Zhao, L. Chen and J. M. Tour, *Org. Lett.*, 2004, ***6***, 2129; (b) Y. Shirai, A. J. Osgood, Y. Zhao, K. F. Kelly and J. M. Tour, *Nano Lett.*, 2005, **5**, 2330; (c) Y. Shirai, A.J. Osgood, Y. Zhao, Y. Yao, L. Saudan, H. Yang, C. Yu-Hung, L. B. Alemany, T. Sasaki, J.-F. Morin, J.M. Guerrero, K. F. Kelly and J. M. Tour, *J. Am. Chem. Soc.*, 2006, **128**, 4854; (d) J.-F. Morin, Y. Shirai and J. M. Tour, *Org. Lett.*, 2006, **8**, 1713.
90 (a) G. Jimenez-Bueno and G. Rapenne, *Tetrahedron Lett.*, 2003, **44**, 6261; (b) G. Rapenne and G. Jimenez-Bueno, *Tetrahedron*, 2007, **63**, 7018.
91 (a) A. Carella, G. Rapenne and J.-P. Launay, *New J. Chem.*, 2005, **29**, 288; (b) A. Carella, C. Coudret, G. Guirado, G. Rapenne, G. Vives and J.-P. Launay, *Dalton Trans.*, 2007, 177; (c) G. Vives, A. Gonzalez, J. Jaud, J.-P. Launay and G. Rapenne, *Chem. Eur. J.*, 2007, ***13***, 5622; (d) Vives, G. Jacquot de Rouville, H.-P. Carella, A. Launay, J.-P. G. Vives, A. Carella, J.-P. Launay and G. Rapenne, *Coord. Chem. Rev.*, 2008, **252**, 1451; (e) G. Vives, H.-P. Jacquot de Rouville, A. Carella, J.-P. Launay and G. Rapenne, *Chem. Soc. Rev.*, 2009, **38**, 1551.
92 G. Vives, A. Carella, S. Sistach, J.-P. Launay and G. Rapenne, *New J. Chem.*, 2006, **30**, 1429.
93 Y. Yu, A. D. Bond, P. W. Leonard, U. J. Lorenz, T. V. Timofeeva, K. P. C. Vollhardt, D. W. Glenn and A. A. Yakovenko, *Chem. Commun.*, 2006, **24**, 2572.
94 V. J. Chebny, D. Dhar, S. V. Lindeman, and R. Rathore, *Org. Lett.*, 2006, **8**, 5041.
95 J. M. Speck, D. Schaarschmidt and H. Lang, *Organometallics*, 2012, **31**, 1975.